

A numerical simulation of tropical storm Chedza over south-eastern Africa

by

Ramontsheng Sakia Rapolaki

Supervisor:

Prof. Chris Reason



Minor dissertation presented in partial fulfilment of the requirements for the degree
of Master of Science in Ocean and Climate Dynamics

Department of Oceanography, University of Cape Town, South Africa

Submitted August 2016

The copyright of this thesis vests in the author. No quotation from it or information derived from it is to be published without full acknowledgement of the source. The thesis is to be used for private study or non-commercial research purposes only.

Published by the University of Cape Town (UCT) in terms of the non-exclusive license granted to UCT by the author.

Plagiarism declaration

I understand the nature of plagiarism, and I am aware of the University's policy on this.

I certify that this minor dissertation reports original work by me during my University project.

Signature:

Signed by candidate

Date August 2016

Signature Removed

Ramontsheng Sakia Rapolaki

Acknowledgements

I am most grateful to my supervisor, Professor Chris Reason, for his invaluable input and support during this project. I am thankful for his constant availability, guidance, assistance and patience. Sincere thanks go to Dr. Raymond Roman, for his assistance with the WRF model setup and all technical related matters. Additional thanks to Mrs. Nadia Jabaar from the Oceanography Department resource centre for her assistance regarding the literature review. A big thanks to my family for their support, and encouragements. I would like to thank the MasterCard Foundation Scholars Program and the University of Cape Town Postgraduate Funding Office for the financial support. The rainfall station data used in this research was kindly provided by the Mozambique Meteorological Institute.

Abstract

Widespread flooding over parts of Malawi, Mozambique, and Madagascar occurred in January 2015. An impact assessment by the World Bank indicated huge damage to property, infrastructure, and agriculture over several regions in south-eastern Africa. The flooding was associated with tropical storm Chedza that developed in the Mozambique Channel on 11 January 2015. This study investigates the atmospheric circulation and potential mechanisms responsible for the heavy rainfall event that occurred between 11 and 17 January over Mozambique and Malawi using the Weather Research and Forecasting (WRF) model, the Global Forecast System (GFS) atmospheric reanalysis, satellite derived rainfall and wind data, and station rainfall data.

Tropical Rainfall Measuring Mission (TRMM) rainfall estimates and rainfall station data indicated that southern Malawi and northern Mozambique experienced the majority of rainfall during the early stages of tropical storm Chedza while Madagascar experienced heavy falls when tropical storm Chedza tracked over the island on January 17. Furthermore, analysis of the station data revealed that the heavy rainfall over Mozambique occurred between 11 and 13 January with some stations recording about 80 % of their total January 2015 rainfall as resulting from this event. The WRF model run of the event indicated a low level easterly to southeasterly onshore flow over southern Mozambique that interacted with a northwesterly monsoonal flow to westerly flow along the northern flanks (periphery) of the storm in the northern Mozambique Channel, leading to surface moisture flux convergence in the regions of heavy rainfall. Furthermore, moisture from the southwest Indian Ocean was advected into the region during the heavy rainfall. It is suggested that multiple favourable factors which included strong moisture fluxes from the southwest Indian Ocean and equatorial South Indian Ocean, near surface convergence

over the areas of heavy rainfall, and strong uplift acted together to create favourable conditions for the development of tropical storm Chedza and the associated heavy rainfall.

Table of contents

Plagiarism declaration	i
Acknowledgements	ii
Abstract.....	iii
Table of contents.....	v
Figure captions and tables.....	vi
List of acronyms.....	ix
1 Introduction.....	1
2 Literature review.....	4
3 Data and methods.....	14
3.1 Station and satellite rainfall data.....	14
3.2 GFS reanalyses data.....	15
3.3 WRF model description and simulations.....	16
3.4 Methods.....	19
4 Results and discussion.....	24
4.1 Synoptic environment and rainfall.....	24
4.2 Modelling Chedza using WRF.....	28
4.3 Contribution of Chedza to rainfall over Mozambique.....	33
5 Conclusions.....	60
References.....	63

Figure captions and tables:

Table 1: Saffir-Simpson scale	13
Table 2: January 2015 total rainfall for various stations over Mozambique divided between northern (in blue font) and southern stations (in black font)	23
Figure 1: Schematic showing primary atmospheric and oceanic features important for rainfall over southern Africa in summer. The symbol L near the source of the cloud band denotes the Angola low, TC denotes tropical cyclones, COLs denotes cut-off low, the cloud bands denote tropical-temperate-troughs, BNino denotes Benguela Niño, and the dotted (purple) line indicates the summer position of the ITCZ (Source: Reason and Smart, 2015).....	12
Figure 2: Map showing southern African countries and the location of the rainfall stations over Mozambique.....	22
Figure 3: Map showing the WRF model domain setup. The symbol 1 refers to the outer domain and 2 refers to the inner domain of the WRF model simulation. The model resolution in the outer domain is 20 km and 6.67 km in the inner domain.....	23
Figure 4: Synoptic charts, produced by SAWS, showing surface conditions over South Africa from (a) 11 to (g) 17 January 2015.....	39
Figure 5: Observed daily rainfall (mm) from 19 stations over Mozambique from 1 to 31 January 2015.....	41
Figure 6: TRMM TMPA daily rainfall (mm) over southern Africa from (a) 11 to (g) 17 January 2015.....	44

Figure 7: 850 hPa geopotential height (m) comparison between WRF simulation (left) and GFS analyses from (a) 14 to (d) 17 January 2015 at 0000 UTC. Contour interval is 20 m.....**45**

Figure 8: 200 hPa geopotential height (m) comparison between WRF simulation (left) and GFS analyses from (a) 14 to (d) 17 January 2015 at 0000 UTC. Contour interval is 20 m.....**47**

Figure 9: 850 hPa wind fields (m s^{-1}) comparison between WRF model simulation (left) and GFS analyses (right) from (a) 14 to (d) 17 January 2015 at 0000 UTC. The arrow in the bottom right of each panel denotes maximum wind speed**49**

Figure 10: Daily surface wind fields (m s^{-1}) comparison between 10-m WRF wind (left) and ASCAT wind (right) from (a) 14 to (d) 17 January 2015. The arrow in the bottom right of each panel denotes maximum wind speed.....**51**

Figure 11: WRF model daily rainfall (mm) over the inner domain from (a) 11 to (g) 17 January 2015.....**53**

Figure 12: WRF model daily moisture flux (shaded, $\text{kg kg}^{-1} \text{m s}^{-1}$) at 850 hPa from (a) 11 to (g) 17 January 2015. Note that for data the values were not plotted at each model grid point. The arrow in the bottom right of each panel denotes the scale which has been used to make the vectors more visible. The actual magnitude of the flux is given in the colour bar.....**54**

Figure 13: WRF model daily moisture flux divergence (shaded, $\text{kg kg}^{-1} \text{s}^{-1}$) at 700 hPa from (a) 11 to (g) 17 January 2015. Negative (positive) values imply convergence (divergence). Note that for data the values were not plotted at each model grid point. The arrow in the bottom right of each panel denotes the scale which has been used to make the vectors more visible. The actual magnitude of the flux is given in the colour bar.....**56**

Figure 14: WRF model daily 500 hPa vertical wind velocity (m s^{-1}) from (a) 11 to (g) 17 January. Only positive values (uplift) were plotted.....**58**

Figure 15: WRF model daily convective instability (°C) calculated between 850 hPa and 500 hPa from (a) 11 to (g) 17 January 2015...**59**

List of acronyms and abbreviations:

AGCMs	Atmospheric General Circulation Models
ARW	Advanced Research WRF
ASCAT	Advanced Scatterometer
DRC	Democratic Republic of the Congo
EUMETSAT	European Organisation for the Exploitation of Meteorological Satellites
GDAS	Global Data Assimilation System
GESDISC	Goddard Earth Science Data and Information Services Centre
GFS	Global Forecasting System
ITCZ	Inter-tropical Convergence Zone
JFM	January February March
MCCs	Mesoscale Convective Complexes
MCSs	Mesoscale Convective Systems
NCAR	National Centre for Atmospheric Research
NCEP	National Centers for Environmental Prediction
NWP	Numerical Weather Prediction
RDA	Research Data Archive

SAHP	South Atlantic High Pressure
SAWS	South African Weather Service
SIHP	South Indian High Pressure
SST	Sea Surface Temperature
TTTs	Tropical Temperate -Troughs
TC	Tropical Cyclone
TE	Tropical-Extratropical
TMI	TRMM Microwave Imager
TRMM	Tropical Rainfall Measuring Mission
UTC	Coordinated Universal Time
WRF	Weather Research and Forecasting
WSM-3	WRF Single-Moment-3 Class
YSU	Yonsei University

Chapter 1

1. Introduction

In January 2015, many regions in south-eastern Africa (southern Tanzania, Malawi, Mozambique, and Malawi) experienced severe floods associated with tropical storm Chedza that developed from a tropical depression over the Mozambique Channel. Table 1 indicates the various categories of tropical disturbances and their associated winds and pressure according to the Saffir-Simpson scale. When compared to the total rainfall recorded for January 2015, Chedza contributed the largest percentage of the monthly rainfall at the coastal stations of Vilanculo, Xai-Xai, Maputo and Mavalane (69%, 70%, 81% and 84% respectively). Substantial contributions also occurred at the inland stations of Montepuez (55%) and Nampula (32%) (Table 2). According to a World Bank report, Chedza left more than 20 000 people homeless and 75 lives were lost along its track in Madagascar. During events such as Chedza, underdeveloped regions with weak economies, such as southern Africa, are often severely impacted. A lack of proper infrastructure to withstand severe weather conditions, poor channels of communication and often a lack of adequate emergency response capacity can lead to significant loss of life. Furthermore, some areas of crops can take a long time to recover from floods, thereby aggravating the adverse impacts of the event.

The occurrence of flood events, or on the other hand, severe droughts over southern Africa is not uncommon. Many studies have shown that southern Africa has a highly variable climate on intraseasonal, interannual, and decadal time scales (e.g. Tyson et al., 1975; Mason and Jury, 1997; Reason and Mulenga, 1999; Behera and Yamagata, 2001; Cook et al., 2004) and is susceptible to heavy floods and severe droughts (e.g. Todd & Washington, 1998; Usman and

Reason, 2004; Reason et al., 2005; Washington and Preston, 2006; Lyon and Mason, 2007). To date however, most of the work has focused on subtropical southern Africa with relatively little effort devoted to tropical storms and associated rainfall impacts over low latitude southern Africa. Therefore, an analysis of tropical storm Chedza, which also had severe impacts in large areas of tropical southern Africa is warranted.

Several studies have shown that severe weather events over southern African often produce heavy rainfall and result in extreme damage to structure and properties (e.g. Dyson and van Heerden, 2001; Reason and Keibel, 2004; Singleton and Reason, 2007; Hart and Reason, 2010; Blamey and Reason, 2012). For example, tropical cyclone Eline of February 2000 contributed about 25 % of the January-February-March (JFM) rainfall over arid to semi-arid southern Namibia (Reason and Keibel, 2004). In addition, Eline left more than 500 000 people homeless in Mozambique and damage caused by floods on roads, bridges, and drainage systems estimated at nearly R880 million (<https://www.dwa.gov.za/hydrology/weather.htm>). This indicates that although some of these events are short-lived (lasting for several hours to a few days) their severe impacts on society and the environment can be long-lasting and highly damaging.

Very few studies exist that have attempted a numerical simulation of a tropical storm in the southern African region. The advantage of a numerical simulation, assuming that it has been validated and is reasonably accurate, is that it may provide useful information that allows one to infer more about the evolution of the storm being modelled and the processes or mechanisms that may have been important. Therefore, this study primarily aims to investigate the heavy precipitation of more than 150 mm within 24 hours that occurred over Mozambique between 11

and 17 January 2015, and to further assess potential atmospheric mechanisms associated with this event using the WRF numerical model. Additionally, the potential influence of tropical cyclone Bansi on the January 2015 heavy rainfall event is also considered. Tropical cyclone Bansi developed on 9 January, over the South Indian Ocean at about 10° S and 65° E, and dissipated on 20 January 2015 at about 45° S and 80° E. Thus, the research objectives are to better understand the evolution of tropical storm Chedza and the heavy rainfall that occurred over the Mozambique region in January 2015 using a combination of WRF model output, GFS reanalyses, station observations, and satellite-derived data sets. Focus is placed on identifying the mechanisms which may have contributed to the heavy rainfall.

This dissertation comprises the following chapters: The literature review on general atmospheric circulation over southern Africa including the main rainfall producing systems and their associated patterns is presented in chapter 2. Data and methodologies are presented in chapter 3. Chapter 4 deals with an analysis of the evolution of tropical storm Chedza, and the observed rainfall from 11 to 17 January 2015 over Mozambique. A WRF model simulation of the event, the regional atmospheric circulation patterns and their roles in creating favourable conditions which led to the high rainfall observed in Mozambique are discussed. The conclusions are presented in chapter 5.

Chapter 2

2. Literature review

Southern Africa has a diverse rainfall regime whose spatial distribution is influenced by multiple factors which include local topography (e.g. Singleton and Reason, 2007), the neighbouring oceans (e.g. Crimp and Mason, 1999; Reason and Mulenga, 1999; Rouault et al., 2003a), distance from the coast and its mean elevation above sea level (e.g. Midgley et al., 2005), and the general atmospheric circulation systems prevailing both in the temperate latitudes to the south and tropics to the north (Tyson and Preston-Whyte, 2015). This section presents a review of southern African summer (December-January-February) climate, the large-scale synoptic rainfall bearing systems over this region and the influences of the regional oceans on the climate.

The general atmospheric circulation over southern Africa is influenced by semi-permanent subtropical high pressures together with the intertropical convergence zone (ITCZ) which shifts latitudinally with seasonal variation (Reason et al., 2006). The Angola low (denoted L in **Fig. 1** at the source of the cloud band) is a tropical semi-permanent shallow heat low over southern Africa. This feature is located over northern Namibia and southern Angola in the lower to mid-troposphere during the summer half of the year (Reason et al., 2006). During its development, the cooler neighbouring oceans and a weak surface high over southern Mozambique help to enhance the pressure gradient across Botswana and Zimbabwe (Hart et al., 2010). The pressure gradient between this heat low and the high pressure sets up a low-level northeasterly flow over the subcontinent.

In summer, the ITCZ shifts southward over south-eastern Africa and strengthens. In February, it is at its southernmost position over central Madagascar and northern Mozambique. Inland from northern Mozambique, the ITCZ forms a meridional arm through the Congo basin before exiting Africa somewhere slightly inland of the Gulf of Guinea (coast) of West Africa. Associated with the ITCZ is a low-level convergence of warm moist air from the Indian Ocean over southern Malawi, northern Mozambique, and central Madagascar. This southward shift and strengthening of the ITCZ is associated with wet summers over the region (southern Africa) while dry summers may result if the ITCZ is weaker or located further north than average (Cook et al., 2004). Moreover, the South Atlantic High Pressure (SAHP) system (**Fig. 1**), moves southeastward during summer to lie closer to the west coast of South Africa leading to an alongshore flow along the west coast. Ridging of the high along the south coast leads to an onshore flow of relatively moist air and forms rainfall along the south and east coasts (Tyson and Preston-Whyte, 2015). Meanwhile, on average the South Indian Ocean High Pressure (SIHP) system moves southeastward in summer favouring the track of frontal systems closer to the southeast of South Africa. These fronts can link up with a tropical disturbance over South Africa to form a Tropical Temperate-Trough (TTT or cloud band), the most important synoptic rain-producing system over southern Africa in summer (Harrison, 1984; Hart et al., 2010) (**Fig. 1**).

Due to its location, southern Africa rainfall is influenced by the Sea Surface Temperature (SST) conditions in the tropical and subtropical Atlantic and Indian Oceans (e.g. Mason, 1995; Reason and Mulenga, 1999; Behera and Yagamata, 2001; Hansingo and Reason, 2009). Historically, more work has been done on the influence of the South Indian Ocean on rainfall patterns over southern Africa and less is known about influence of the South Atlantic Ocean (Reason et al.,

2006). However, recent studies have shown a possible relationship between the Atlantic Ocean and rainfall over southern Africa. Several studies have indicated the northern Angola-Benguela region over the tropical south-eastern Atlantic as another source of moisture flux associated with rainfall over southern Africa (Rouault et al., 2003a; Manhique et al., 2015; Reason and Smart 2015).

Previously, Hansingo and Reason (2009) suggested a possible link between rainfall over southern Africa and the tropical South Atlantic Ocean. These authors showed that during occurrence of positive SST anomalies in the southeast Atlantic Ocean as well as the southwest Indian Ocean, parts of south-eastern Africa experienced enhanced rainfall. Recently, Manhique et al. (2015) studied the relationship between rainfall and SST during austral summer to explain the devastating flood event over central and southern Mozambique of January 2013. Their study revealed positive SST anomalies of about 1 to 2 °C over the southeast Atlantic Ocean in the region known as the Benguela Niño (**Fig. 1**) during the event as well as warm SSTs in the southwest Indian Ocean. It was suggested that these SST anomalies were favourable for the contribution of low-level moisture flux convergence over the southern Mozambique region that led to period of severe rainfall during January 2013, consistent with the model results of Hansingo and Reason (2009).

On the other hand, a significant amount of work has been done on the influence of the Indian Ocean on the climate and weather of southern Africa (e.g. Mason 1995; Reason and Mulenga, 1999; Behera and Yamagata, 2001; Reason, 2001, 2002; Washington and Preston, 2006). The

semi-permanent South Indian Ocean anticyclone, positioned east of southeast of South Africa, advects moisture into the South African region (Tyson and Preston-Whyte, 2015). Further south, large amounts of heat fluxes are released to the overlying atmosphere above the Agulhas retroflection and Agulhas Return Current which may strengthen cold fronts tracking here and help form the midlatitude component of the TTT (Walker and Mey, 1998; Reason, 2001; Rouault et al., 2003b). A number of studies (e.g. Mason, 1995; Reason and Mulenga, 1999; Behera and Yamagata, 2001; Reason, 2001) have shown increased summer rainfall over large areas of subtropical southern Africa.

2.1 Main rainfall producing systems over southern Africa

TTTs are cloud bands that result from tropical-extratropical (TE) interactions (Hart et al., 2010). According to Harrison (1984) and Reason et al. (2006), TTTs are the primary rain bearing weather systems during austral summer over subtropical southern Africa (i.e. south of 15°S). TTTs can be identified as cloud bands that stretch over southern Africa in a southeast to northwest direction and usually extending (NW-SE) from the Angola heat low, as illustrated in **Fig. 1**. Importantly, these systems are associated with moisture and heat transport from tropical southwest Indian Ocean to mid-latitudes (Reason et al., 2006). This transport results in high precipitation rates over southern Africa (Hart et al., 2010). These authors found that a TTT event of 1997/1998 January contributed more than 40 % of the rainfall over large areas of South Africa for November-February season.

Additional systems that often led to heavy rainfall over southern Africa are Mesoscale Convective Systems (MCSs). MCSs are made up of an organised group of thunderstorms acting as coherent systems, which include Mesoscale Convective Complexes (MCCs) and squall lines (Blamey and Reason, 2012). These systems can last longer than 12 hours. Using TRMM TPMA (Multi-satellite Precipitation Analysis) data to study precipitation caused by the MCCs over southern Africa during the period 1998 to 2006, Blamey and Reason (2012) found out that on average, about nine MCC events per year occur over southern Africa. Furthermore, MCCs contribute up to 20 % of summer rainfall in places over the eastern part of southern Africa. This percentage decreased to less than 6 % over the western interior. Furthermore, individual MCCs can produce more than 100 mm of rainfall within a 24-hour period while some produce about a third of the total monthly rainfall (Blamey and Reason, 2013). However, the mechanism behind MCCs formation is still not well understood.

Cut-off lows may also significantly contribute to rainfall over South Africa and the southern parts of Mozambique and Madagascar, particularly during the transition seasons. Cut-off lows are defined as cold cored systems that have been cut-off from the main westerly flow and displaced equatorward of the polar jet stream (Taljaard, 1985; Singleton and Reason, 2007; Nieto, et al., 2008). A major characteristic of cut-off lows is that their development is strongly linked to the occurrence of a strong ridge of high pressure located south of South Africa over the South Atlantic Ocean. Furthermore, these systems are often associated with intense rainfall and stratosphere-troposphere exchange (Barsby and Diab, 1995; Singleton and Reason, 2007; Nieto et al, 2008). Taljaard's (1985) ten year (1973-1982) study of cut-off lows over the South African region bounded between 20° and 38°S indicated that on average, 11 cut-off lows occurred over

South Africa per year. Singleton and Reason (2007) conducted an extended study over 30 years (1973-2002) to form a climatology of cut-off lows over subtropical southern Africa. The monthly climatological frequency of cut-off lows from the study revealed least occurrences during December and January, and high frequencies for March, April, May, and June, with April being the most common month for cut-off lows over subtropical southern Africa. On occasion, these systems can produce more than 100 mm of rainfall in 24 hours.

Tropical cyclones in the region (denoted TCs in **Fig. 1**) are low-pressure systems with a well-developed eye in the tropical Indian Ocean (Tyson and Preston-Whyte, 2015). Usually, tropical systems form during summer over the South Indian Ocean, with between six and twelve recorded every year with, the southwest Indian Ocean tropical cyclone season typically as between November and April (Malherbe et al., 2012; Malan et al., 2013). On average, 10 to 12 of the tropical depressions mature to tropical cyclones over the southwest Indian Ocean (Jury et al., 1999; Malherbe et al., 2013; Malan et al., 2013). Although some tropical cyclones are generated in the Mozambique Channel, not all of these make landfall, instead they may track south through the Channel (Reason, 2007). Of those generated in the southwest Indian Ocean, about 5 % make landfall on the southern African mainland (Nash et al., 2015). Mavume et al. (2009) showed that about 48 of 64 TCs occurring during the period 1980 to 2007 made landfall over Madagascar, thus making this region the most vulnerable to southwestern Indian Ocean tropical cyclones. Malherbe et al. (2012) indicated that the contribution of tropical systems to annual rainfall over the southern interior of southern Africa is less than 10%, but when they occur they are often associated with extreme, devastating floods.

Henderson-Sellers et al. (1998) indicated that the following factors are believed to be significant for tropical cyclone formation: i) favorable atmospheric conditions e.g. increased low-level relative vorticity, ii) conditional instability through a deep atmospheric layer, iii) increased relative humidity values in the lower and middle atmosphere, iv) weak vertical wind shear, v) a deep oceanic mixed layer, and vi) SST above 26° C. Each stage in the development of a tropical cyclone is characterized by a certain pressure and wind speed at that particular event as listed in Table 1.

While tropical cyclones are associated with heavy rainfall, the precursor tropical storms can also lead to large amounts of precipitation. Such was the case with Chedza, studied here, which produced floods in some areas but neither developed from a landfalling tropical cyclone nor developed into one when it tracked across the Mozambique Channel.

A significant amount of work has been done on the genesis and tracks of southwest Indian Ocean tropical cyclones over the past years (e.g. Mavume et al., 2009; Astier et al., 2012; Fitchett and Grab, 2015). However, a better understanding of the mechanisms that may contribute to heavy rainfall and floods during tropical storms is still crucial. Rain-bearing circulation systems do not always result in large rainfall amounts. The moisture fluxes, extent of atmospheric instability and the divergence field under any condition determines the amount of rainfall produced (Tyson and Preston-Whyte, 2015). For instance, weak surface convergence coupled with upper-level divergence which does not provide an adequate uplift in stable air will only lead to cloud formation without precipitation (Tyson and Preston-Whyte, 2015). For precipitation to occur, strong surface convergence coupled with upper-level divergence is needed to produce adequate uplift in conditionally unstable air. Heavy rains result from all these factors acting together in a strongly unstable air mass at a particular time and space.

Most of the above-mentioned weather systems can produce large amounts of rainfall within a few hours of their genesis, and thus using high-resolution data is necessary for tracking and monitoring their associated impacts. Unfortunately, there are no high-resolution data over Mozambique and Malawi other than what can be inferred from satellite observations such as TRMM or GFS re-analyses. Therefore, it is useful to see whether a high-resolution regional atmospheric model (WRF) can adequately represent the large scale aspects of a tropical storm. Assuming that the WRF simulation can do this, then it can be applied towards investigating the circulations patterns that may lead to heavy rainfall. In this dissertation, this approach is used to better understand tropical storm Chedza and its associated heavy rainfall over Mozambique and southern Malawi.

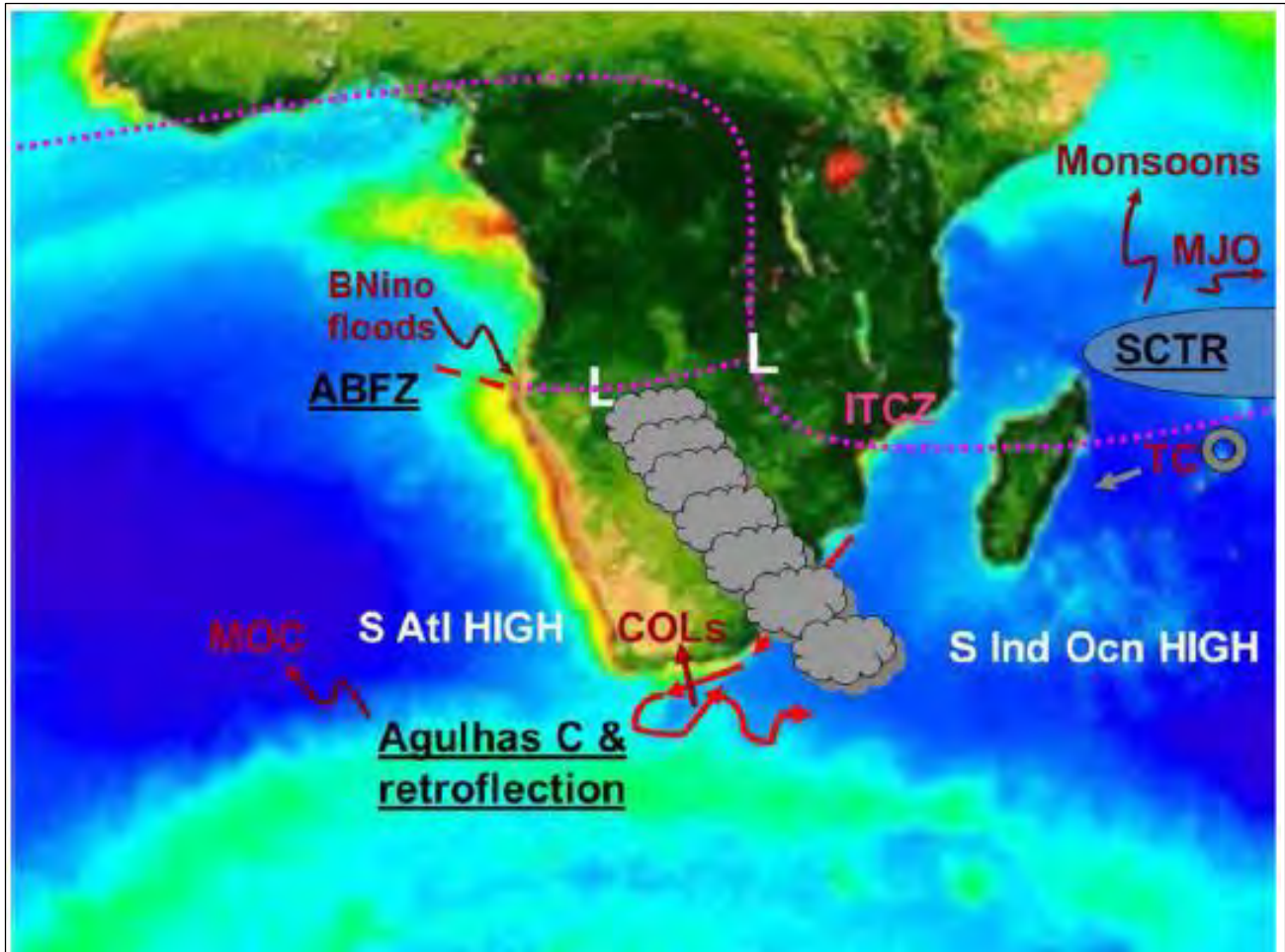


Figure 1: Schematic showing primary atmospheric and oceanic features important for rainfall over southern Africa in summer. The symbol L denotes the Angola low near the source of the cloud band, TC denotes tropical cyclones, COLs denotes cut-off low, the cloud bands denote tropical-temperate troughs, BNino denotes Benguela Niño, and a dotted (purple) line indicates the summer position of the ITCZ (Source: Reason and Smart, 2015).

Table 1: Saffir-Simpson scale (Source: <http://www.nhc.noaa.gov/aboutsshws.php>)

Type	Category	Pressure (mb)	Winds (mph)	Wind (kmph)	Surge (m)
Tropical Depression	TD	-----	< 39	< 62	----
Tropical Storm	TS	-----	39-73	63-118	----
Tropical Cyclone	1	> 980	74-95	119-153	1.2-1.5
Tropical Cyclone	2	965-980	96-110	154-177	1.6-2.4
Tropical Cyclone	3	945-965	111-130	178-209	2.5-3.6
Tropical Cyclone	4	920-945	131-155	210-250	3.7-5.4
Tropical Cyclone	5	<920	>155	>250	>5.4

Chapter 3

3. Data and methods

3.1 Station and satellite data

Hourly rainfall data from 19 stations in Mozambique were provided by the Mozambique Meteorological Office (as depicted in **Fig.2**). The daily time series were produced for the period 1 to 31 January 2015. The rainfall contribution of the storm was represented as the percentage contribution to the total January rainfall recorded at each station (**Table 2**). The purpose was to show the quantity of rainfall over Mozambique from 11 to 17 January 2015 and the impact of the storm in terms of rainfall. Unfortunately, it was not possible to get daily rainfall data from Malawi or Madagascar.

To show the extent of the rainfall distribution over south-eastern Africa from 11 to 17 January 2015, daily rainfall composite maps over southern Africa were computed from the three hourly TRMM satellite estimates. The TRMM satellite uses a Microwave Imager (TMI) instrument whose passive remote sensing occurs at low altitudes of around 402 km and helps resolve rainfall equatorward of about 40°. The horizontal resolution of TRMM is 0.25° x 0.25° (Lin et al., 2012). The TRMM dataset is useful for the analysis of rainfall associated with severe storms events, particularly over southern Africa which is a mainly data sparse region with a limited rain gauge network. Previous studies have found that TRMM products generally match the daily patterns fairly well (Rouault et al., 2010). However, the TMI sensor aboard the satellite tends to overestimate rainfall over the tropics, mainly during the warm season (Nesbit et al., 2004; Ebert

et al. 2007; Jiang et al., 2008). TRMM data was downloaded from Goddard Earth Science Data and Information Services Centre (GESDISC) website: <http://disc.sci.gsfc.nasa.gov>.

The Advanced Scatterometer (ASCAT) was used in this present study to evaluate the WRF model near-surface winds. ASCAT is an active sensor on board Meteorological Operation-A (MetOp-A) satellite that was launched by European Organisation for the Exploitation of Meteorological Satellites (EUMETSAT) MetOp-A satellite in October 2006 (Figa-Saldana et al., 2002; Bi et al., 2011). The sensor retrieves vector winds over the ocean surface. The ASCAT data used in this study has a spatial resolution of 25 km. The daily ASCAT data was downloaded from the Physical Oceanography Distributed Active Archive Centre (PODAAC) website: <https://podaac.jpl.nasa.gov/dataset/ASCATB-L2-25km>.

3.2 GFS reanalyses data

The GFS model reanalyses data was used in this study to provide initial boundary conditions for the WRF model (Lin et al., 2010). GFS is a coupled weather prediction model developed by the National Centers for Environmental Prediction (NCEP) (Kalney et al., 1996). The GFS model is made up of four separate models (an atmosphere model, an ocean model, a land/soil model, and a sea ice model) which interact to give an accurate forecast of weather conditions. The horizontal resolution of GFS is (0.5° X 0.5°) and it has assimilated data from aircraft, upper air soundings, and satellite observations. The boundary conditions for GFS are provided by the Global Data Assimilation System (GDAS) generated from multiple satellite and surface observations. The GFS model is initialized at four times per day (0000, 0600, 1200, 1800 UTC). Furthermore, its

six hourly land surface, oceanic, and atmospheric forecasts are available at 0.2, 0.5, 1.0, and 2.5-degree horizontal resolution archived on Research Data Archive (RDA) website: (<http://rda.ucar.edu/datasets/ds083.2/>).

3.3 WRF model description and simulations

Significant progress has been made in numerical simulations of tropical cyclones due to improvements in computing power and advancements in observational data used to force the models. However, fine resolution models are too costly for most research groups with limited computational resources (Kim et al., 2015). In the past, Atmospheric General Circulation Models (AGCMs) with relatively coarse resolution have often been used to study tropical cyclones. These models tend to underestimate the intensity of tropical storms and poorly simulate their main properties such as track, genesis location, and central pressure minima. For regional models, uncertainties in choosing model physics parameterizations and initial conditions are still a challenge that leads to errors in the simulation (Cha and Wang, 2012). Cha and Wang (2012) suggest that one way to improve tropical cyclone simulations is by improving initial conditions, resolution, and model physics. In this study, the WRF model was used to simulate tropical storm Chedza. The model physics, resolution, and boundary conditions were selected carefully based on previous studies (e.g. Noh et al., 2003; Hong and Lee, 2009; Lin et al., 2010; Ibrahim and Afandi, 2014; Nguyen et al., 2014; Islam et al., 2015) so as to minimise the errors in the simulation as discussed below.

WRF is a fully compressible, terrain-following (sigma) coordinate and non-hydrostatic model on an Arakawa-C grid, developed by the National Centre for Atmospheric Research (NCAR)

(Skamarock et al., 2005). The WRF model is designed to be a flexible state-of-the-art atmospheric simulation system suitable for a broad range of applications such as idealised simulations, data assimilation research, parameterization research, and real-time numerical weather prediction (NWP) (Skamarock et al., 2008). The model was chosen for this study as it is freely available and has been used extensively for simulation and analyses of tropical cyclones (e.g. Hill and Lackmann, 2009; Cha and Wang, 2012; Kim et al., 2015). The version used in this study is Version 3.6.1 with the Advance Research (ARW) dynamic solver in which a Runge-Kutta 2nd and 3rd order time integration techniques are used for model integration. The model has both one and two-way nesting capabilities to allow for the interaction between the mother and child domain.

For this study, the simulation used two-way nested domains so that the processes and circulation simulated in the inner domain were fed back into the lower resolution outer domain (model domains are depicted in **Fig. 3**). The parent domain had 20 km horizontal resolution while the child domain had 6.67 km resolution. The parent domain had 418 x 246 grid points with 20-km grid spacing, and a time step of 180 seconds. The child domain had 880 x 523 points with 6.67-km grid spacing, and a time step of 60 seconds. Both domains were initialized at 0000 UTC 10 January and ran until 2300 UTC 20 January 2015. The outer domain was chosen in such a way that it covers the southern African region (5°N to 45°S, 0°E to 85°E) including the southeast Atlantic and southwest Indian Oceans. The inner domain covered the track of tropical storm Chedza and neighbouring ocean (3°S to 36°S, 10°E to 70°E). Both domains had 30 vertical levels between the surface and the model top at 50 hPa. The model was set up to produce six-hourly averages in order to use the same time scale as the GFS reanalyses data. The model was

allowed a 24-hour spin-up period and the output was analysed from 0000 UTC 11 January 2015. GFS reanalyses data were used for initialization and boundary conditions. Daily high-resolution ($0.5^\circ \times 0.5^\circ$) (Reynolds et al., 2007) optimally interpolated SST was used to provide the lower boundary conditions for the simulation (Kim et al., 2015). SST during 11-17 January period in the Mozambique Channel and immediately east of Madagascar was close to its climatological value (not shown).

The physics options used for model runs included the WRF Single-Moment3-class (WSM3) simple ice microphysics scheme (Hong et al., 2006) on the outer domain (20 km) and WSM6-class graupel scheme in the inner domain (6.67 km) for cloud microphysics (Hong et al., 2004). This scheme comprises of ice, snow, and graupel processes suitable for high-resolution simulations (Kumar et al., 2008). The Kain-Fritsch (new Eta) cumulus parameterization scheme (Kain, 2004) was used for convective processes as it is suitable for simulation of precipitation in mesoscale models (Hong and Lee, 2009; Ibrahim and Afandi, 2014). The Dudhia shortwave radiation scheme (Dudhia, 1989), Yonsei University (YSU) planetary boundary layer scheme (Noh et al., 2003), and the Noah land surface model scheme were used to represent land surface processes. The performance of the WRF model and its ability to simulate circulation patterns associated with tropical storm Chedza is evaluated through a comparison of winds and geopotential height simulated by the WRF model and GFS reanalyses (described above).

3.4 Methods

a. WRF model validation

The ability of the WRF model to reproduce the characteristics of tropical storm Chedza and regional atmospheric patterns is investigated by comparing the model atmospheric circulation with GFS analyses and satellite data sets (TRMM TMI and ASCAT). For validation of pressure fields and wind patterns, the WRF model geopotential height, and u and v wind vectors were interpolated onto 200 hPa, 700 hPa, and 850 hPa pressure levels.

Model winds and geopotential height patterns were then compared with the GFS analyses patterns at 850 hPa and 200 hPa pressure levels for 14-17 January. The 850 hPa level was chosen because it is just above the height of the interior plateau and it is a convenient level to analyse circulation patterns over the interior of southern Africa (Reason and Smart, 2015). The 200 hPa level was chosen to see if the model was able to reproduce the upper anticyclonic flow (divergence) at the top of the storm.

For validation of surface wind, the WRF model u and v wind vectors at 10 m level (above the sea surface) were compared to daily ASCAT satellite derived winds from 14 to 17 January. This was to assess how well the model can reproduce the winds over the ocean surface. In addition, the ability of the model to simulate rainfall patterns associated with tropical storm Chedza was validated against TRMM TMI satellite derived rainfall. The model does not contain total rainfall in its output list. Total rainfall (t_rain) was calculated from:

$$t_rain = precip_g + precip_c \dots\dots\dots(1)$$

where *precip_c* (mm) is the accumulated total cumulus precipitation and *precip_g* (mm) is the accumulated total grid-scale precipitation.

b. Moisture flux and its convergence, uplift, and instability

To investigate the regional atmospheric mechanisms that may have contributed to the flood event that occurred between 11 and 17 January over Mozambique, the moisture flux, its convergence (negative values in the divergence field), vertical velocity, and convective instability were examined over the inner domain (6.67 km resolution). The moisture flux divergence at 700 hPa (expressed in kg kg⁻¹ s⁻¹) was computed using the following variables obtained from the WRF model; specific humidity *q* (kg kg⁻¹), and the horizontal wind components *u,v* (m s⁻¹) at that level. The individual *qu* and *qv* components were combined to give a moisture flux vector, which has both direction and magnitude. The magnitude (*Q*) of the vector was calculated from:

$$Q = \sqrt{(qu)^2 + (qv)^2} \dots\dots\dots(2)$$

Moisture flux divergence is given by:

$$\text{Moisture flux divergence} = (\partial qu / \partial x) + (\partial qv / \partial y) \dots\dots\dots(3)$$

where $\partial qu / \partial x$ is the change in zonal moisture flux over longitude and $\partial qv / \partial y$ is the change in the meridional moisture flux over latitude. The moisture flux divergence was plotted over the region 5°S to 35°S and 15°E to 60°E to determine the locations of strong convergence (negative values in the divergence field). Moisture flux vectors were used to indicate the source of moisture during the event.

To show areas of strong uplift associated with rainfall and cloudiness during the event, daily plots of vertical velocity over the inner domain were computed at 500 hPa for 11 to 17 January 2015. Negative (positive) values of vertical velocity indicate subsidence (uplift). Also, convective instability ($^{\circ}\text{C}$) was used to show areas of strong instability associated with the event (Singleton and Reason, 2007). Instability was calculated as the magnitude of the temperature difference between potential temperature ($\theta_{850} - \theta_{500}$) at 500 hPa and 850 hPa.

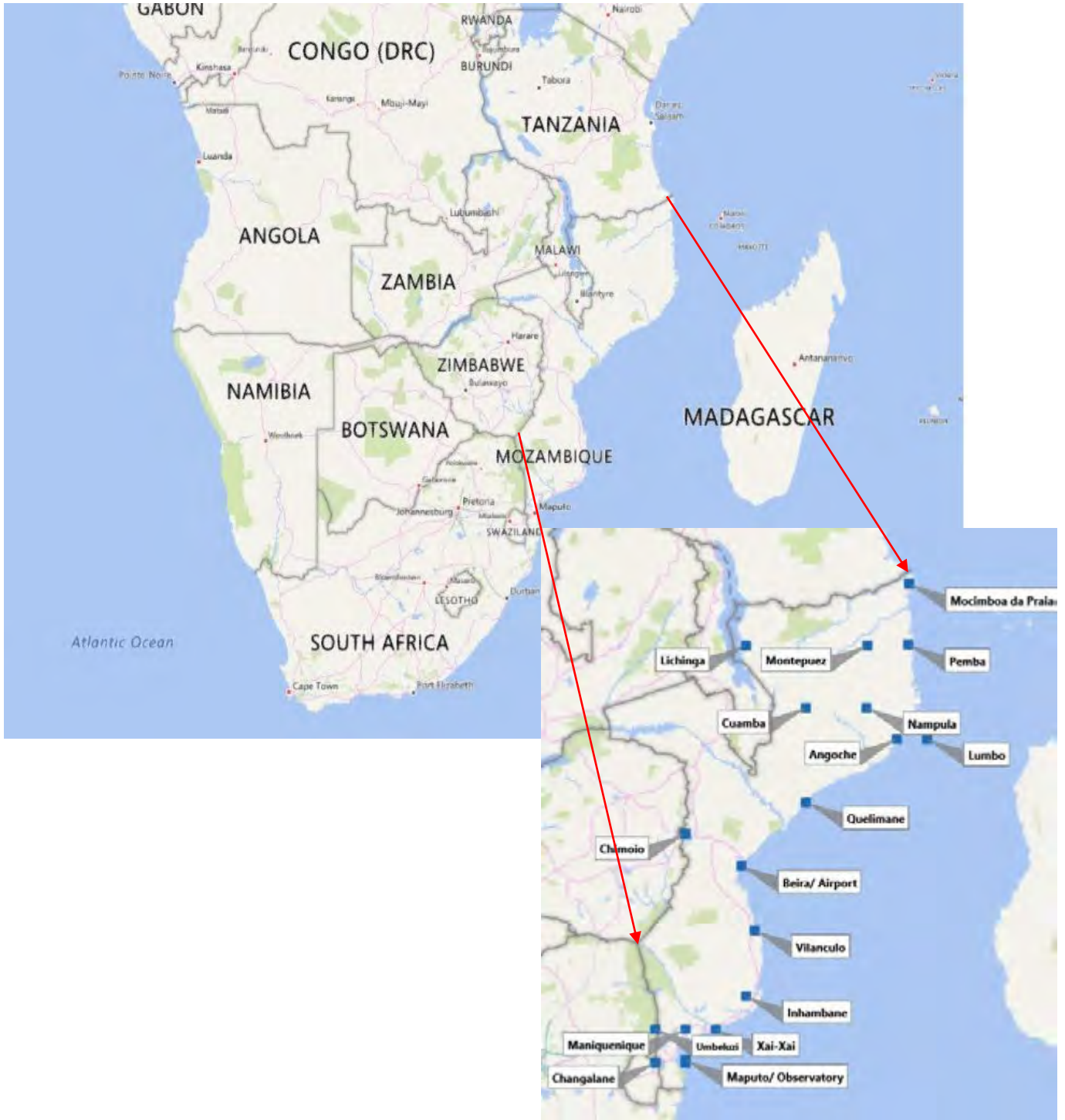


Figure 2: Map showing southern African countries and the location of the rainfall stations over Mozambique.

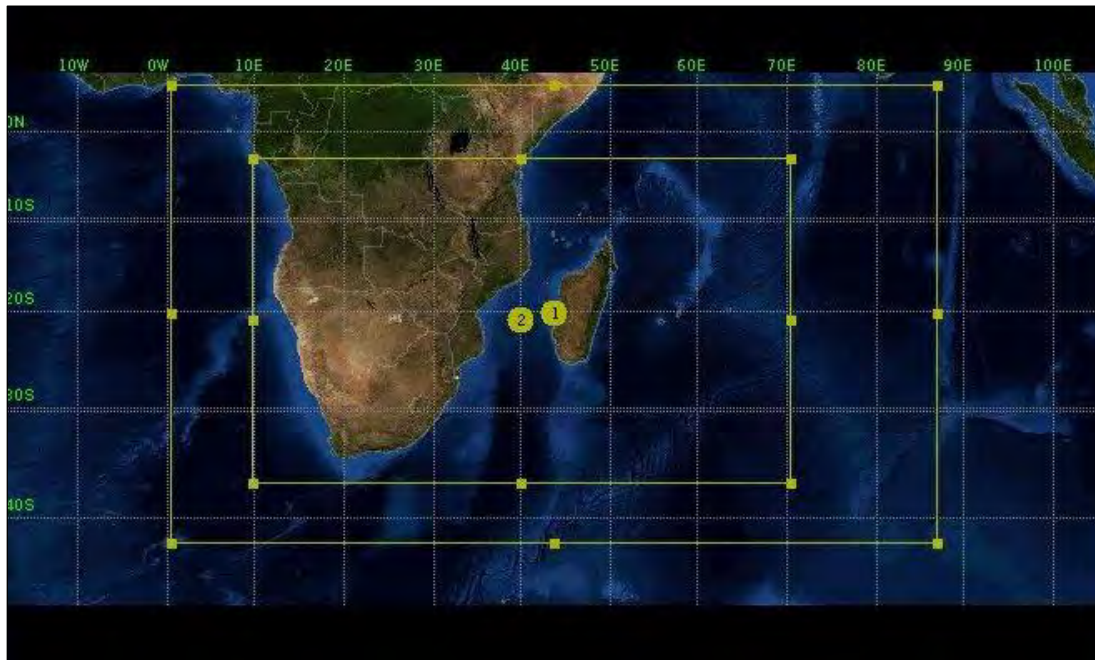


Figure 3: Map showing the WRF model domain setup. The symbol 1 refers to the outer domain and 2 refers to the inner domain of the WRF model simulation. The model resolution in the outer domain is 20 km and 6.67 km in the inner domain.

Table 2: January 2015 total rainfall for various stations over Mozambique divided between northern (in blue font) and southern stations (in black font).

Station	Lat	Lon	January total (mm)	Storm contribution (mm)	Storm % contribution
Pemba	-12.97	40.375	384.2	203.8	53.0
Mocimboa da Praia	-11	40.4	238.1	118.6	49.8
Montepuez	-13	39.03	536.5	295.6	55.1
Lichinga	-13.0	35.0	390.1	114.5	29.4
Lumbo	-16	41	208.9	40.5	19.4
Cuamba	-15	37	619.9	304.6	49.1
Nampula	-15	37	414.8	130.7	31.5
Angoche	-16	40	231	86.7	37.5
Quelimane	-18	37	436.7	140.8	32.2
Chimoio	-19.0	33.0	135.4	4.1	3.0
Beira/Airport	-20	34.85	83.2	54.6	65.6
Maputo/Observatory	-26.0	33.0	59.3	48.1	81.1
Xai-Xai	-25	34	78.9	55	69.7
Inhambane	-24	35	76.5	15.7	20.5
Vilanculo	-22	35.3	66.1	45.4	68.7
Umbeluzi	-25	32	24.3	13.6	56.0
Maniquenique	-25.0	33.0	67.3	28.1	41.8
Changalane	-26	32	10.3	6.4	62.1
Maputo/Mavalane	-25.92	33	130.5	110	84.3

Chapter 4

4. Results and discussion

4.1 Synoptic environment and rainfall

This section looks at the evolution of tropical storm Chedza from its initiation stage to its dissipation stage. Chedza developed over the Mozambique Channel on 11 January 2015 as a tropical depression and was upgraded to a named tropical storm (Chedza) on 15 January. **Fig. 4** shows the South African Weather Service (SAWS) surface synoptic charts from 11 to 17 January 2015. The chart for 11 January shows tropical storm Chedza in its early developmental stage as a tropical depression with a central isobaric pressure of 1004 hPa located in the northern part of the Mozambique Channel, centred near 17°S, 42°E (**Fig. 4a**). Tropical lows were located over northern Namibia and northern Zimbabwe/ southern Zambia with a trough over central South Africa. An eastward moving cold front was situated southwest of South Africa over the South Atlantic Ocean. The other significant feature to notice at this time was the trailing edge of a midlatitude anticyclone situated south-east of South Africa (near 38°S, 40°E), leading to a southeasterly onshore flow over the east coast.

The presence of the tropical depression in the northern Mozambique Channel and its associated onshore flow led to several stations in northern Mozambique (Pemba, Mocimboa da Praia, Angoche) recording about 50 mm or more on this day (**Fig. 5**). The TRMM rainfall satellite estimate for this day shows a band of relatively strong rainfall extending from southern Malawi to the north coast of Mozambique (**Fig. 6a**). Another region of heavy rainfall was located east of Madagascar over the tropical Indian Ocean associated with tropical cyclone Bansi. Over northern

Mozambique, TRMM estimated a rainfall maximum of up to 140 mm whereas the wettest rain gauge station was Angoche (68 mm).

By 12 UTC 12 January (UTC refers to Coordinated Universal Time), the tropical depression in the northern part of the Mozambique Channel had moved slightly west to lie on the north coast of Mozambique near 18°S, 38°E (**Fig. 4b**). An interior low-pressure system was situated over northern Botswana and the trough over South Africa had extended to the south coast of South Africa. These low-pressure systems over the northern Botswana and Angola may have played a role in some areas over tropical southern Africa receiving widespread rainfall on this day (**Fig. 6b**). Moisture convergence driven by the developing Chedza in the northern Mozambique Channel and strong ridging in southwest Indian Ocean led to heavy rainfall in parts of northern Mozambique and southern Malawi. **Fig. 5** shows that Cuamba, located near the Malawi/Mozambique border received 190 mm consistent with the TRMM estimate (**Fig. 6b**) of about 150 mm in this area. TRMM shows a band of heavy rainfall extending from Malawi eastward across northern Mozambique as well as in the Mozambique Channel and over Madagascar.

On 13 January, the tropical depression deepened to below 1000 hPa but had moved only slightly southeast of its position the previous day (**Fig 4c**). Meanwhile, the ridge in the South Indian Ocean shifted northward blocking the depression (Chedza) from moving southward. A large low was located over Botswana and neighbouring areas. Cuamba again received the heaviest rainfall of about 70 mm on this day, with nearby Nampula receiving about 55 mm (**Fig. 5**). The TRMM estimate showed widespread rainfall of about 40-80 mm over southern Malawi and northern Mozambique near the location of Cuamba. More intense rainfall was indicated by TRMM in the

eastern southern Mozambique Channel near (20°S, 45°E) (**Fig. 6c**). The highest rainfall values in TRMM are found to the east of Madagascar (>160 mm) in the region of tropical cyclone Bansi.

On 14 January, Chedza was located near 19°S, 39°E in the northern part of the Mozambique Channel (**Fig. 4d**). The low over Botswana had moved to be centred over the border with Zambia and the ridge in the southwest Indian Ocean had merged with the ridging anticyclone from the South Atlantic Ocean to form a strong anticyclone south of Madagascar. The presence of this anticyclone in the southwest Indian Ocean at the surface might have prevented Chedza from moving south, out of the Channel, similar to what happened with tropical cyclone Dera in 2001 (Reason, 2007). In terms of rainfall, Mavalane station near Maputo received the highest rainfall of about 70 mm on this day, while several stations experienced dry conditions (**Fig. 5**). TRMM showed widespread rainfall over Zambia, northern Mozambique, and southern Tanzania with largest amounts over the south-eastern part of the Mozambique Channel (near 20°S, 44°E) (**Fig. 6d**). A small area of rainfall of about 60-80 mm was evident near the border of KwaZulu-Natal and southern Mozambique, consistent with the 70 mm recorded at Mavalane station.

Chedza continued to intensify as it tracked eastward across the Mozambique Channel toward Madagascar on 15 January and achieved named tropical storm status. The synoptic chart for this day shows the system located west of Madagascar (near 18°S, 45°E) (**Fig. 4e**) with a central pressure of less than 992 hPa. There were lows situated over southern Botswana/ Northern Cape and over the south coast with the South Atlantic High ridging over western South Africa. The trailing edge of the anticyclone in the southwest Indian Ocean remained more or less in the same position as the previous day blocking the southward movement of Chedza. The other prominent

surface features on this day included a tropical low located over southern Zambia/ northern Zimbabwe, creating favourable conditions for rainfall over Zambia and Angola (**Fig. 6e**). The TRMM data also indicated rainfall near the lows over South Africa as well as over northern Mozambique and partially along the west coast of Madagascar. Several stations in northern Mozambique experienced rainfall (**Fig. 5**) with Lumbo (32 mm) being the wettest (**Fig. 5**). Further south, Xai-Xai (47 mm) received the most rainfall but this is not captured in the TRMM (**Fig. 6e**).

On 16 January, Chedza strengthened further and moved further east to centre itself just offshore of the coast of southwestern Madagascar (near 20°S, 42°E) (**Fig. 4f**). The South African Weather Service issued a warning for a severe tropical storm in the Mozambique Channel on this day. The trailing edge of the high in the southwest Indian Ocean had moved slightly east but it still discouraged southward movement of Chedza. Over western South Africa, the ridging high extended further inland and along the south coast with a cold front and a coastal low located over the Eastern Cape and southern KwaZulu-Natal coasts respectively. **Fig. 6f** shows the rainfall along the south and east coasts of South Africa estimated by TRMM. Heaviest rainfall is indicated over western and southern Madagascar associated with Chedza. **Fig. 6f** also indicates widespread rainfall over Angola, Zambia and the southern Democratic Republic of the Congo (DRC) associated with the large low located over Botswana and southern Zambia. Most Mozambican stations recorded little or no rainfall (**Fig. 5**) consistent with the TRMM estimate of mainly dry conditions (**Fig. 6f**).

On 17 January, tropical storm Chedza weakened substantially and was downgraded to a tropical depression with a central pressure of about 1002 hPa. Its location was hardly different to the previous day. However, rainfall remained heavy with totals of around 100 to 120 mm over northern Madagascar and extreme values of around 200 mm on the south-east of the island in the TRMM estimate (**Fig. 6g**). The passage of the cold front just to the east of Maputo favoured tropical temperature trough formation and substantial rainfall over some coastal station such as Xai-Xai (45 mm) and Vilanculo (**Fig. 5**).

This section has described the evolution of Chedza and other important synoptic features during the week of heavy rainfall over large parts of Mozambique, Malawi and Madagascar which caused severe flooding and damage in areas. In order to obtain greater insight into Chedza, the WRF model is now used to simulate the storm. The next section compares various circulation and wind fields with GFS analyses and satellite winds. Although WRF is nudged to GFS at its outer domain (**Fig. 3**), it is free to evolve away from that boundary whereas the GFS analyses assimilate all available observations throughout the domain.

4. 2 Modelling Chedza using WRF

a. Validation

The WRF Model was initialized at 00 UTC 10 January and ran until 23 UTC 20 January with two-way nested grids of 20 and 6.67 km horizontal resolution respectively. Both domains were centred at 20°S, 40°E in the Mozambique Channel and had 30 σ -levels between the surface and

50 hPa. Default topography (similar to Flesch and Reuter, 2012) was used for both domains. Geopotential height and wind fields were interpolated onto 200 and 850 hPa pressure levels.

Fig. 7 shows the daily sequence of 850 hPa geopotential height over the outer domain at 0000 UTC for 14-17 January 2015 from the WRF simulation (left) and from GFS analyses (right) while **Fig. 8** are the same plots but at 200hPa. Both sequences of plots show Chedza evolving in the Mozambique Channel and tropical cyclone Bansi to the east of Madagascar near 55-60°E. However, the intensity of the two cyclones is stronger in WRF, particularly in the case of Chedza. Furthermore, the WRF run shows a third cyclone to the east of Bansi near the eastern boundary of the domain. This feature is not evident in the GFS analyses except as a weak trough at 200 hPa on 15 and 16 January (**Fig. 8a-b**). In WRF, this system is weak at upper levels and by 17 January, it has tracked to the far east of the domain as is also the case in GFS. Other synoptic scale features in **Fig. 7** are similar in WRF and GFS although the anticyclone south-east of South Africa and the trough passing south of South Africa on 15-16 January (**Fig. 7c-d**) have a slightly greater magnitude in the former.

Fig. 9 shows the daily sequence of 850 hPa winds for 14-17 January from the WRF simulation and GFS analyses over the outer domain at 00 UTC. Chedza was located in the central Mozambique Channel (centred near 18°S, 39°E) with tropical cyclone Bansi to the east of Madagascar (near 55°E) on January 14th (**Fig. 9a**). Although the synoptic patterns are very similar, there are noticeable differences between WRF and GFS in the magnitude of the winds. Also, GFS shows a single large tropical cyclone (Bansi) east of Madagascar whereas WRF resolves two smaller cyclones. However, it seems conceivable that the GFS winds in Bansi are

too weak since this cyclone was a category 4 system at this stage (Mawren and Reason, 2016). The maximum wind in GFS is 194 km hr^{-1} (54 m s^{-1}) whereas WRF shows maximum winds in Bansi of 264 km hr^{-1} (73 m s^{-1}). The 850 hPa winds in Chedza are also somewhat stronger in WRF compared to GFS. However, the wind speeds at 200 hPa are more comparable (not shown). In addition, the low-level winds over the land are weaker in WRF, likely due to the higher resolution which captures small scale orography and vegetated areas better than GFS and hence has greater surface friction. Furthermore, the convergence between the tropical south-easterly winds and the north-westerly monsoonal winds in the WRF occurs slightly further south than in the GFS analyses.

At 00 UTC 15 January, Chedza had moved slightly east to lie near 41°E and Bansi was located near 60°E and near maximum intensity (category 5, Mawren and Reason, 2016) (**Fig. 9b**). The other synoptic scale features are comparable between WRF and GFS. However, the WRF maximum winds in Bansi strengthened to 269 km hr^{-1} (75 m s^{-1}) compared to the previous day. On the other hand, the GFS winds weakened to a maximum of 170 km hr^{-1} (47 m s^{-1}) on this day. The weak cyclone east of Bansi near 70°E shown in WRF was not present in GFS at this time, which only showed a single large tropical cyclone. As described below and shown in Fig. 10, the satellite altimeter winds (ASCAT) did resolve a weak cyclone east of Bansi suggesting that the WRF simulation is more accurate than GFS in this respect. Both models display similar strength winds in the cold front approaching to the south-west of Cape Town on this day.

At 00 UTC 16 January, WRF shows tropical storm Chedza situated near $19^\circ\text{S}, 40^\circ\text{E}$ compared to $19^\circ\text{E}, 41^\circ\text{E}$ in GFS (**Fig. 9c**) with WRF simulating stronger winds. Again, WRF resolves two

cyclones east of Madagascar with the largest, Bansi, located near 62°E whereas GFS has a single larger tropical cyclone located near 65°E.

At 00 UTC 17 January, both WRF and GFS show a single tropical cyclone east of Madagascar but this system is further north and west in WRF compared to GFS. Over the southern Mozambique Channel, WRF shows Chedza located over the southwest coast of Madagascar similar to the synoptic chart (**Fig. 4g**) whereas GFS places it further west over south-eastern Madagascar and with a much reduced magnitude.

The daily WRF model winds at 10 m over the outer domain (20 km) are now verified against 0.25° (25 km) ASCAT wind observation for 14-17 January 2015 (**Fig. 10a-d**). Unlike GFS, ASCAT shows evidence of a weak additional cyclone east of Bansi on January 14 similar in location to WRF (**Fig. 10a**). However, Chedza is positioned slightly further south in the Mozambique Channel (near 19°S, 39°E) in the WRF run. Furthermore, the model shows maximum winds in Bansi of 123 km hr⁻¹ (34 m s⁻¹) while ASCAT shows a maximum wind of 110 km hr⁻¹ (30 m s⁻¹). Throughout the sequence until 16 January, there is general agreement between WRF and ASCAT in the locations of Chedza and Bansi but there are differences in wind strength. A major difference between the WRF simulated wind and ASCAT satellite derived fields appears on 17 January, and in particular in the position of the cyclones (**Fig. 10d**). Chedza is located further south (about 5°) over the south-west coast (near 25°S, 45°E) of Madagascar in WRF whereas ASCAT implies that it is located a few hundred kilometres further north.

Although it is known that regional model simulations of rainfall are problematic, it is of interest to see whether the WRF rainfall patterns are broadly similar to those estimated by TRMM. Examination of the daily sequence in **Figs. 6** and **11** show that the broad patterns are in agreement. There is more fine-scale structure in the WRF rainfall, consistent with its higher resolution (~7 km), compared to TRMM (~50 km). Another difference is that WRF tends to show greater rainfall in the tropical regions than TRMM whereas over the ocean areas south of South Africa the reverse is the case. In terms of the former, WRF has significantly greater rainfall associated with Chedza and Bansi than TRMM does, except on 15 January over the west coast of Madagascar (**Figs 6e, 11e**).

To summarise, the WRF model showed some differences from GFS in the position and strength of the cyclones, particularly in simulating the position of tropical storm Chedza, but the evolution of the systems was reproduced accurately. WRF simulates the storm to generate in approximately the same location as the GFS analysis on the 14 January, and the simulated position of the storm closely matches the GFS analysis until 16 January, after which the simulated storm does not move over Madagascar unlike GFS. There is also a difference in the location of Chedza in WRF compared to ASCAT on 17 January. However, prior to this day, WRF and ASCAT were in relatively good agreement. The broad scale rainfall patterns in WRF and TRMM are similar although there are some differences in magnitude. In general, however, the differences are small enough that there is confidence in using WRF to better understand the evolution of Chedza and its associated rainfall, as presented below.

4.3 Contribution of Chedza to rainfall over Mozambique

As discussed above, there was a significant rainfall over Mozambique and Malawi associated with Chedza. Focus is placed on understanding the rainfall over Mozambique rather than over Malawi or Madagascar since station rainfall data was only available for Mozambique. This section aims to understand the circulation patterns and mechanisms during tropical storm Chedza that may have led to the heavy rainfall over Mozambique. The 850 hPa WRF model moisture flux, its convergence at 700 hPa, 500 hPa vertical velocity, and the convective instability calculated between 850 hPa and 500 hPa pressure levels, are used to help understand the observed rainfall in TRMM satellite and the WRF model run over Mozambique between 11 and 17 January 2015.

Fig. 12 shows daily 850 hPa moisture fluxes for 11-17 January. At 00 UTC on the 11th, the centre of Chedza was in the narrowest part of the Mozambique Channel slightly south of the island station of Lumbo. The strongest moisture fluxes were located just to the southwest of the centre in an onshore flow towards Angoche which received about 70 mm on this day (the wettest for the period) (**Fig. 5**). The 700 hPa divergence pattern shows an area of convergence with a maximum of $-6 \times 10^{-6} \text{ kg kg}^{-1} \text{ s}^{-1}$ over Angoche (17-18°S, 37-39°E) (**Fig. 13a**). A prominent region of uplift was evident over the coastal region near Angoche and also on the eastern periphery of the cyclone (**Fig. 14a**). These areas of marked uplift more or less match up with those of substantial satellite derived rainfall (**Fig. 6a**) and WRF rainfall (**Fig. 11a**). Further north from Angoche, the coastal station of Pemba experienced far less rainfall (**Fig. 5**) (5mm) since the flow here was offshore. However, at the coastal station Mocimboa da Praia, near the

Mozambican / Tanzanian border, there was convergence between the cyclonic flow associated with Chedza and the monsoonal northwesterlies leading to about 50 mm of rainfall at this station. The TRMM rainfall estimate shows a band of relatively strong rainfall extending north and northwest of this station over south-eastern Tanzania (**Fig. 6a**). The WRF model rainfall over the inner domain (6.67 km) shows a similar band of strong rainfall to TRMM (**Fig. 11a**). Furthermore, regions of relatively strong convective instability indicative of an unstable lower and midlevel troposphere (**Fig. 15a**) were evident over Mozambique, where the heavy rainfall was observed.

In the model, Chedza made landfall during the day on the 11th and by 00 UTC on the 12th, its centre was situated inland, about 100 km west of Angoche, near 16°S (**Fig. 12b**), where strong uplift was evident (**Fig. 14b**) and heavy rainfall in both the TRMM estimate (**Fig. 6b**), and the WRF run occurred (**Fig. 11b**). There was ongoing moisture flux convergence (**Fig. 13b**) between the monsoonal northwesterlies and the offshore flux in the north so Mocimboa da Praia and an inland station about 150 km to its southwest, Montepuez, each received about 30 mm on this day. These stations lie within the band of rainfall observed over the coast of northern Mozambique in TRMM and WRF (**Figs. 6b, 11b**). However, by far the wettest station on the 12th was Cuamba, located near the border with Malawi and about 200 km west northwest of Angoche, where about 190 mm was recorded (**Fig. 5**). Cuamba also lies close to the centre of the heaviest rain in the TRMM data (**Fig. 6b**). **Figs. 12b** and **13b** indicate that Cuamba was situated in a region of strong south-easterly moisture flux and convergence. This flux impacted moisture on the local topography leading to the heavy rainfall there. It was also in a region of enhanced uplift (**Fig. 14b**) and strong convective instability (**Fig. 15b**). Another inland station, Nampula

which lies about halfway between Cuamba and the coast, received 50 mm whereas, Montepuez experienced about 25 mm on this day. On the coast, Mocimboa de Praia recorded about 25 mm and Quelimane, near 18°S and located near the strongest onshore fluxes received about 30mm (**Fig. 5**).

At 00 UTC on the 13th, Chedza was located over the Mozambican coastline with its centre just to the northeast of Quelimane, near 18°S, and with relatively strong southeasterly moisture fluxes over central Mozambique (**Fig. 12c**). Bands of strong uplift were present near the coast at Quelimane and also inland over southern Malawi and extending towards Cuamba (**Fig. 14c**). There was a strong moisture flux convergence at 700 hPa near Quelimane as well as near southern Malawi (**Fig. 13c**). Cuamba was also the wettest station on this day (about 70 mm) while Lichinga, to its north, experienced about 40 mm (its wettest day of the period). A band of relatively heavy rainfall can be seen in the TRMM estimate extending north from near Quelimane towards Cuamba and Malawi (**Fig. 6c**) while WRF shows a broader rainfall band (**Fig. 11c**). The onshore moisture fluxes evident in **Fig. 12c** resulted in substantial rainfall (15-25 mm) at the coastal stations of Maputo, Beira, Quelimane and Pemba, although strong uplift can only be seen near Quelimane and Pemba (**Fig. 14c**). However, most of Mozambique shows relatively high levels of convective instability on this day (**Fig. 15c**).

At 00 UTC on the 14th, Chedza was located well offshore of the Mozambican coast leading to onshore moisture flux towards Angoche (**Fig. 12d**). The main areas of moisture flux convergence were near the centre of Chedza (**Fig. 13d**) although some areas of convergence existed near the coast. The model shows strong uplift in the region of Chedza extending towards

the coast near Angoche (**Fig. 14d**), large regions of convective instability (**Fig. 15d**), and heavy rainfall in these areas (**Fig. 11d**). TRMM, however, only shows substantial rainfall over the Mozambique Channel and the west coast of Madagascar (**Fig. 6d**). Interestingly, the wettest station on the 15th was the island of Lumbo (35 mm) (**Fig. 5**), located about 50 km offshore from Angoche and located in a region of relatively heavy rain according to TRMM and WRF (**Fig. 11d**).

On the 15th, TRMM indicates little rainfall over Mozambique except in the north (**Fig. 11e**) although some stations further south received notable fall (**Fig. 5**). WRF shows a large area of rainfall over central to northern Mozambique (**Fig. 11e**). WRF rainfall near the Mozambican coast at about 18-20°S can be matched with areas of uplift (**Fig. 14e**) and moisture flux convergence (**Fig. 13e**) and convective instability (**Fig. 15e**). However, it is less obvious what is behind the widespread WRF rainfall further north over Mozambique. Heaviest rainfall is evident on the southern flanks of Chedza where there is strong moisture flux convergence (**Fig. 13e**) and uplift (**Fig 14e**). Moisture associated with Chedza was able to penetrate well inland, the inland station of Umbeluzi (near the South African border) received almost 10 mm of precipitation on this day although this is not obvious in the TRMM estimate.

Chedza tracked slowly east-southeastwards during the 15th, so by 00 UTC on the 16th, its centre was still in the middle part of the Channel near 41°E. Rainfall recorded on the 16th was much reduced compared to previous days with only Pemba and Maputo observing substantial rainfall (**Fig 5**). These wet areas can also be seen in the TRMM data (**Fig. 6f**). However, WRF continued to show heavy rain over northern Mozambique (**Fig. 11f**) which seems inconsistent with TRMM

and the station data. Strong uplift and moisture flux convergence in the model was only obvious in the central and eastern Mozambique Channel (**Fig. 14f**) where both TRMM and show relatively heavy rain (**Fig. 6f**).

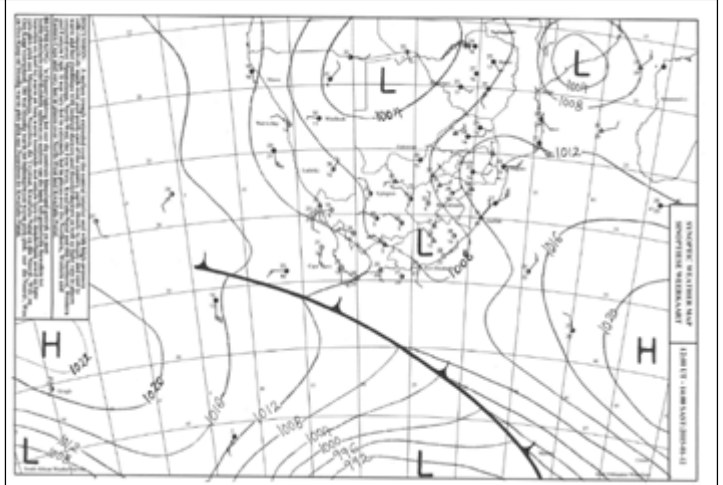
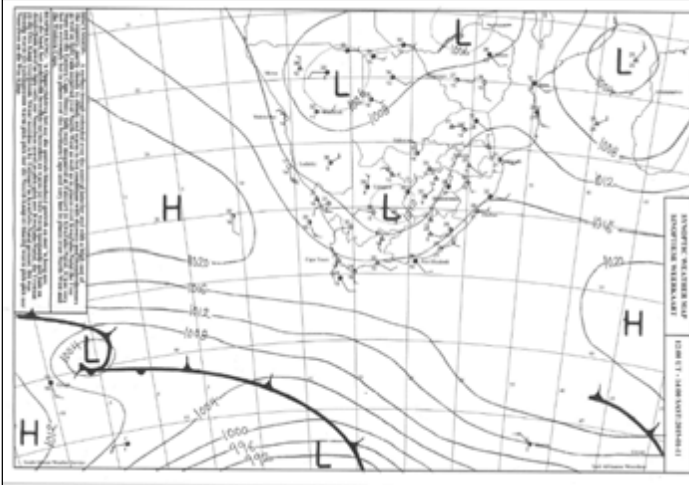
During the 16th, Chedza's track became more southeastward in direction and by 00 UTC on the 17th, it had made landfall on the southwestern coast of Madagascar (near Toliara) with its centre slightly offshore (**Figs. 6g** and **11g**). Onshore moisture fluxes prevailed along the central Mozambican coastline south of about 22° S, with several coastal stations receiving sizeable rainfall amounts on this day (**Fig. 5**) although the mid-tropospheric uplift here was relatively weak (**Fig. 14g**). However, examination of the South African Weather Service synoptic charts for this day indicates that this rainfall over southern Mozambique resulted from a relatively weak tropical temperate trough that formed between a weak low situated over Zimbabwe and a cold front passing south-east of South Africa. TRMM also showed regions of relatively heavy rainfall over southern Mozambique on the 17th but, its heaviest falls occurred just east of the eastern periphery of Chedza near the high orography of southern Madagascar (**Fig. 6g**) whereas WRF showed heaviest rainfall further west. A strong area of moisture flux convergence (**Fig. 13g**), uplift (**Fig. 14g**) and convective instability (**Fig. 15g**) were apparent in WRF over the areas of heavy rainfall in southwestern Madagascar (**Fig. 11g**).

In summary, examination of the WRF fields suggests that the main areas of substantial rainfall are consistent with those in low-level moisture flux convergence, mid-level uplift, and high convective instability. The model results imply that moist low-level air advected by Chedza together with the presence of an unstable air mass over Mozambique throughout the period

helped to produce the rainfall over central and northern Mozambique and southern Malawi. Convergence of the southeasterly flow in the Mozambique Channel with the monsoonal north westerlies over northern Mozambique/southern Tanzania also contributed to the rainfall in those regions. Similar processes operated in western Madagascar while the pronounced orography of that island also played an important role during the 15-17 January as the low-level moisture flux associated with Chedza impacted in those mountains.

(a)

(b)



(c)

(d)

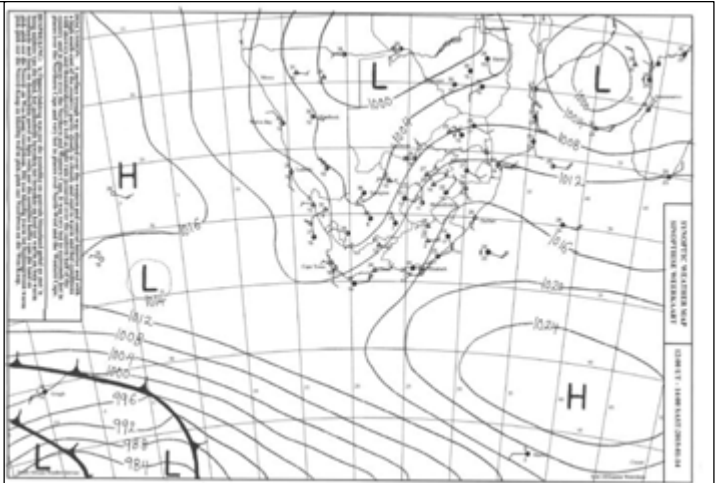
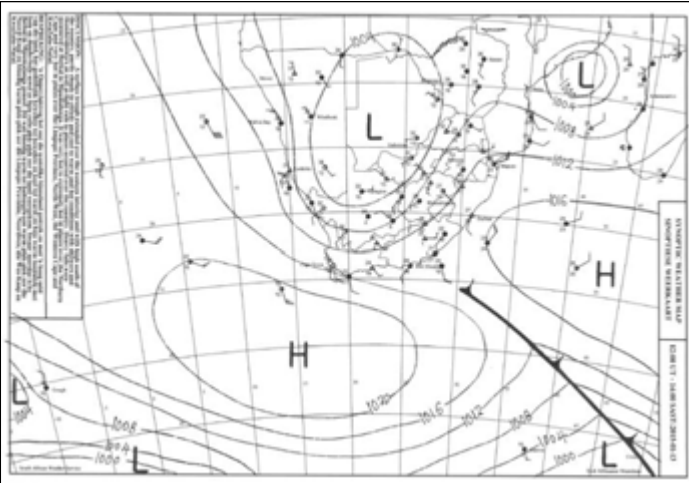
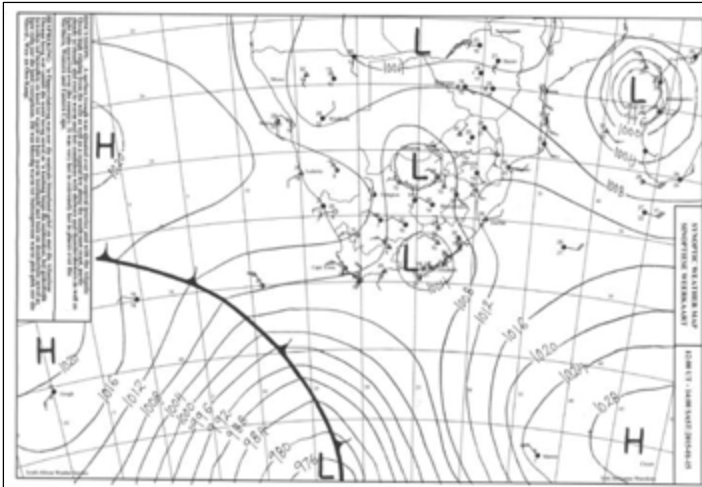
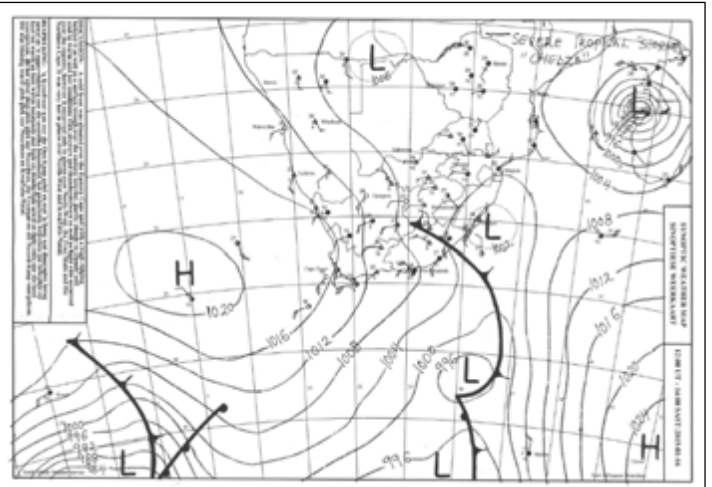


Figure 4: Synoptic charts, produce by SAWS, showing surface conditions over southern Africa from (a) 11 to (g) 17 January 2015 (Continued on next page).

(e)



(f)



(g)

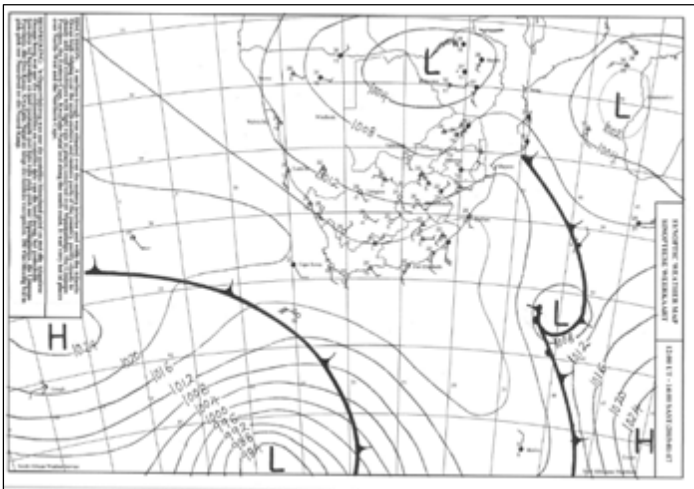


Figure 4: (continued) Synoptic charts, produce by SAWS, showing surface conditions over southern Africa from (a) 11 to (g) 17 January 2015.

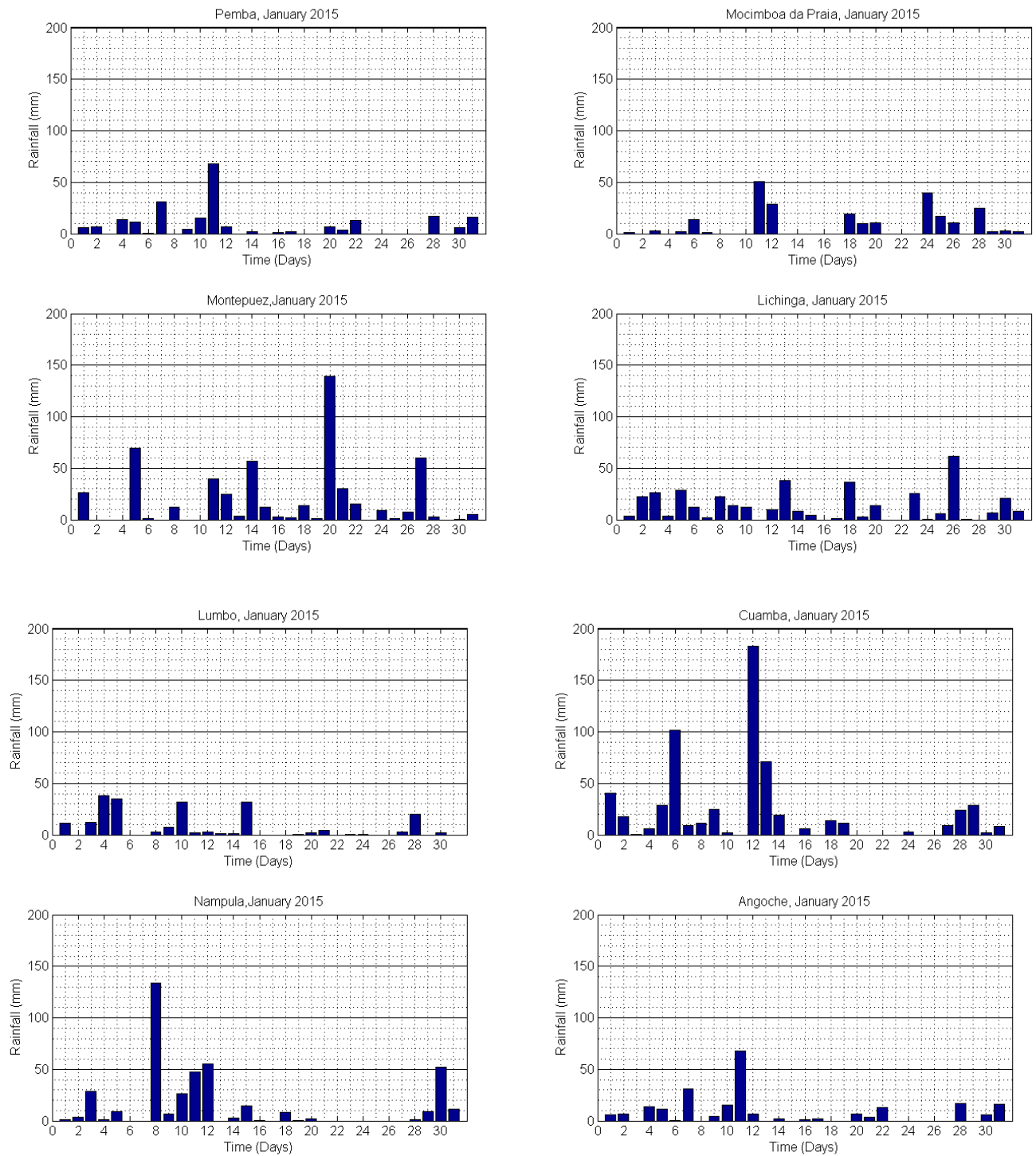


Figure 5: Observed daily rainfall (mm) from 19 stations over Mozambique from 1 to 31 January 2015 (Continued on next page).

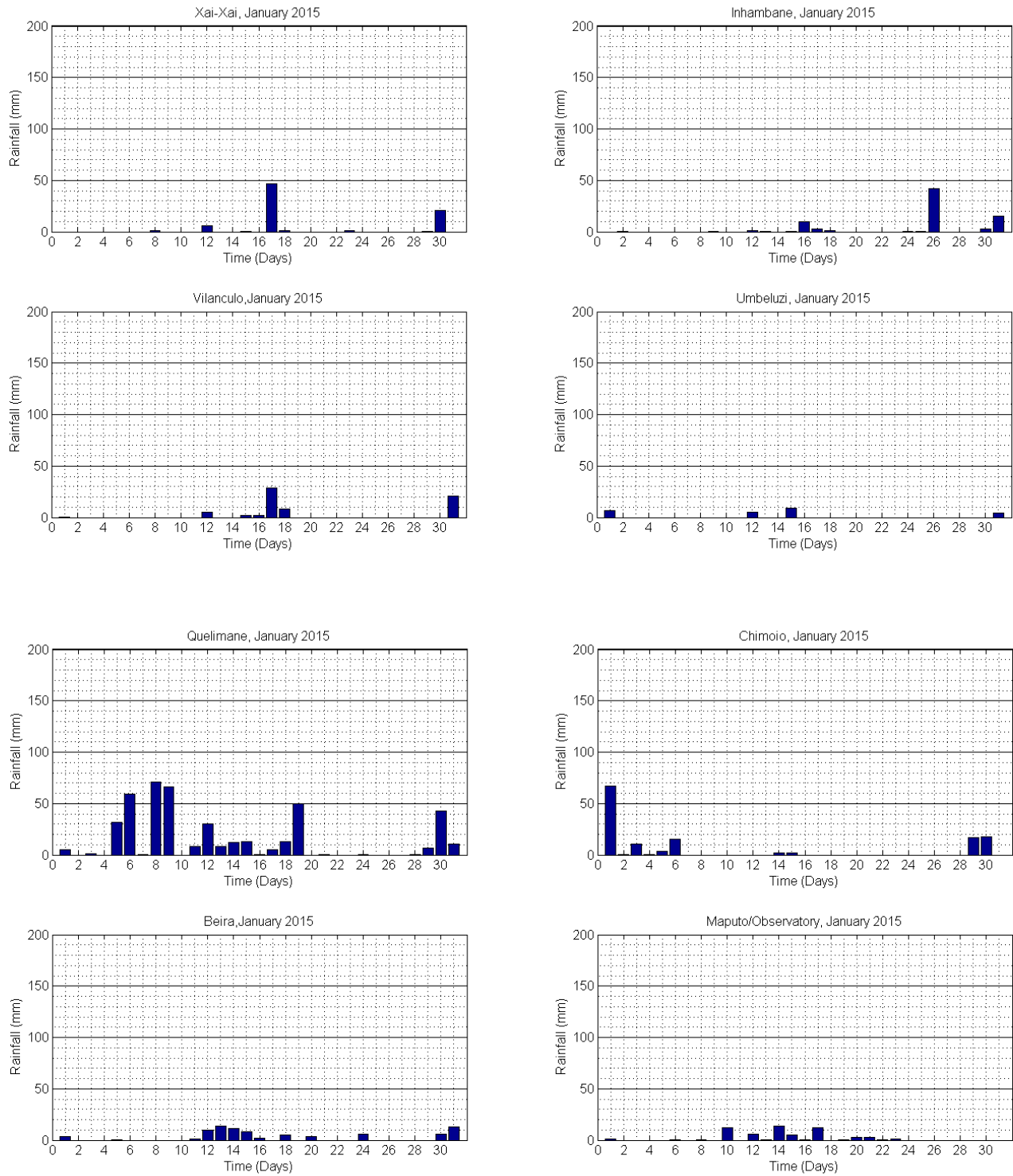


Figure 5: (Continued) Observed daily rainfall (mm) from 19 stations over Mozambique from 1 to 31 January 2015.

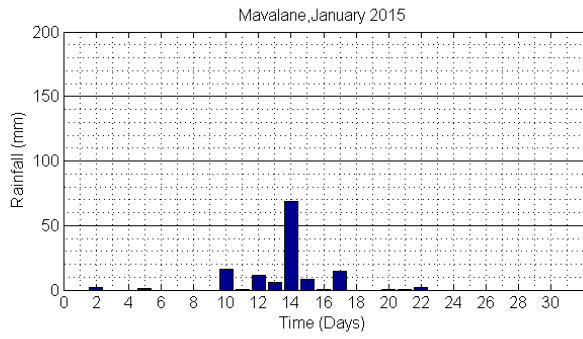
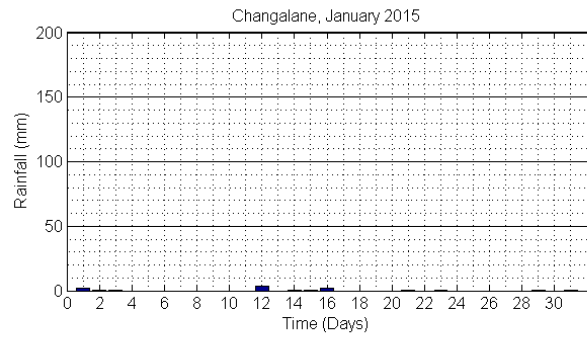
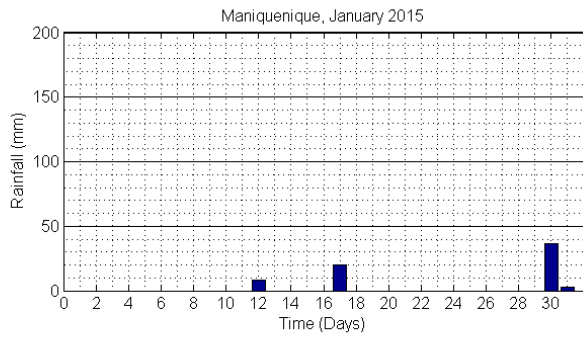


Figure 5: (Continued) Observed daily rainfall (mm) from 19 stations over Mozambique from 1 to 31 January 2015.

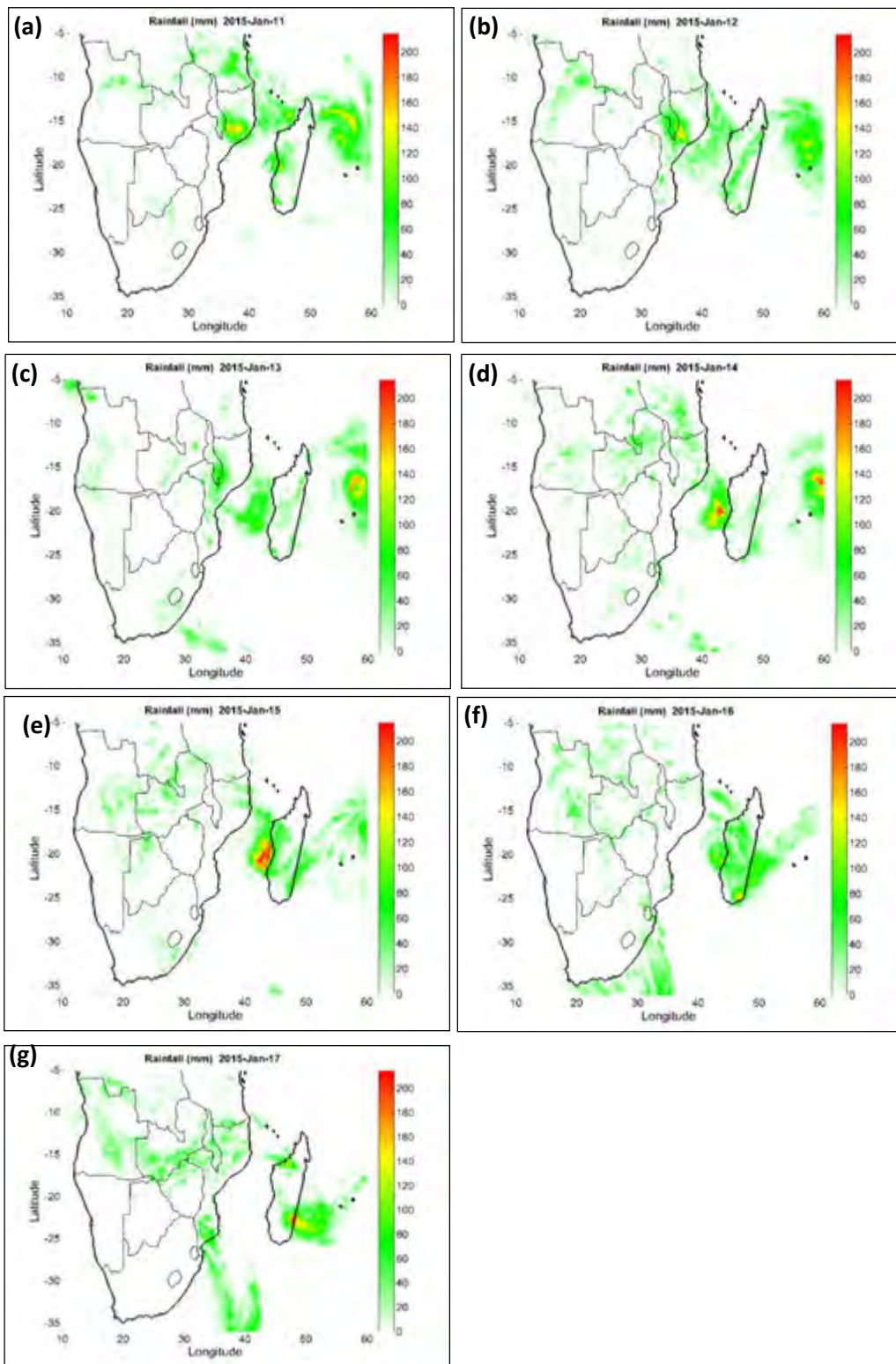


Figure 6: TRMM TMPA daily rainfall (mm) over southern Africa from (a) 11 to (g) 17 January 2015.

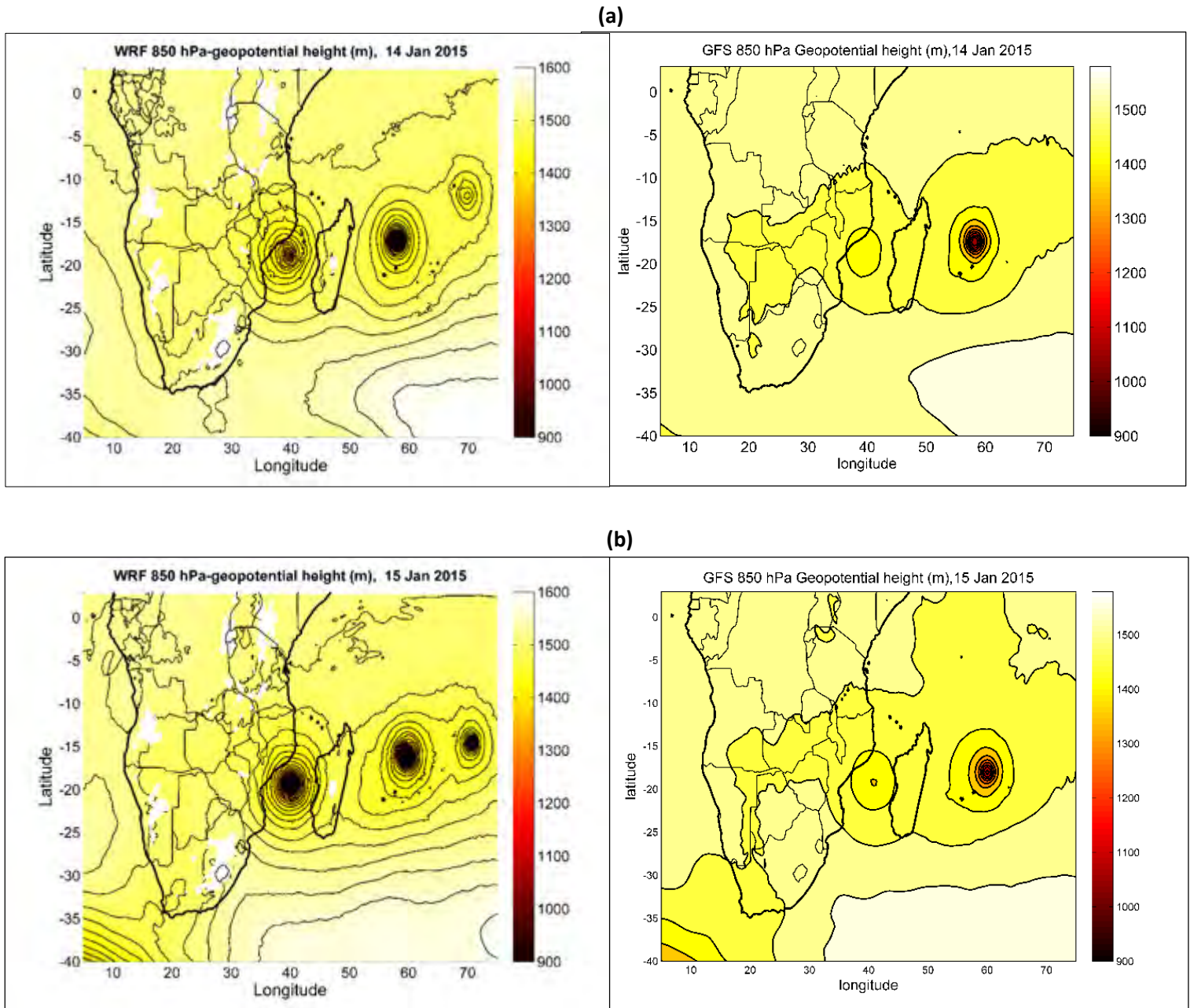
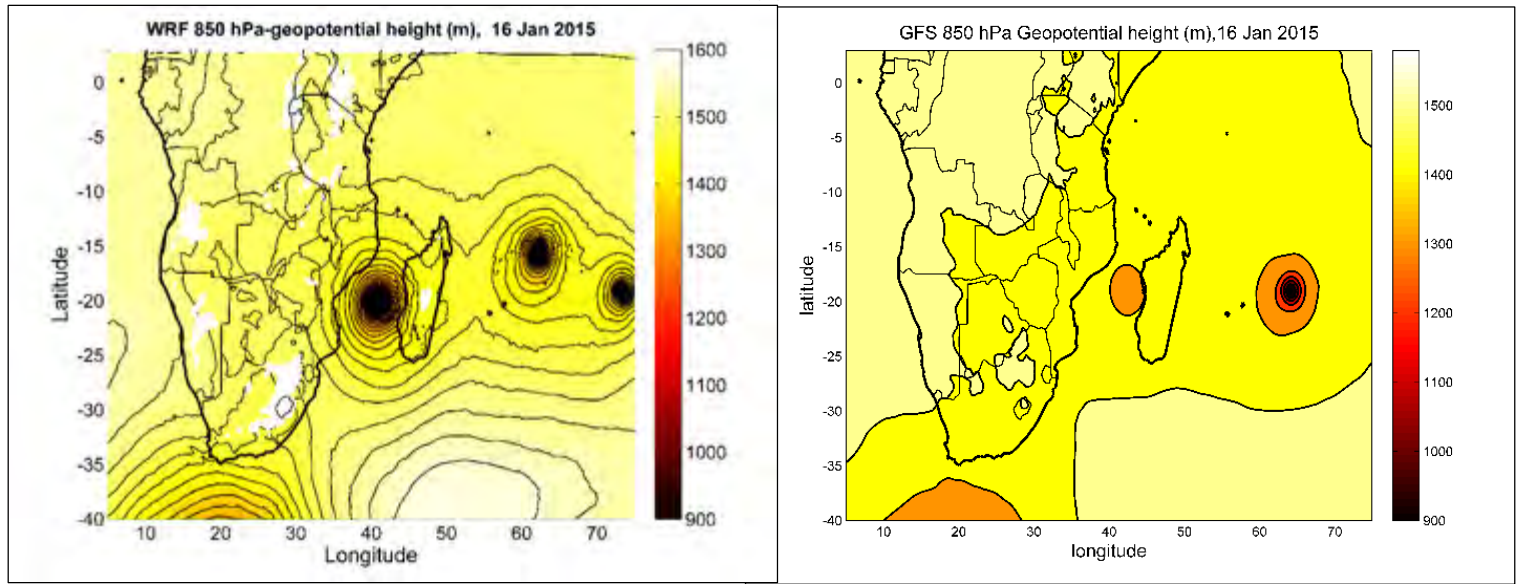


Figure 7: 850 hPa geopotential height (m) comparison between WRF simulation (left) and GFS analyses from (a) 14 to (d) 17 January 2015 at 0000 UTC (Continued on next page). Contour interval is 20 m.

(c)



(d)

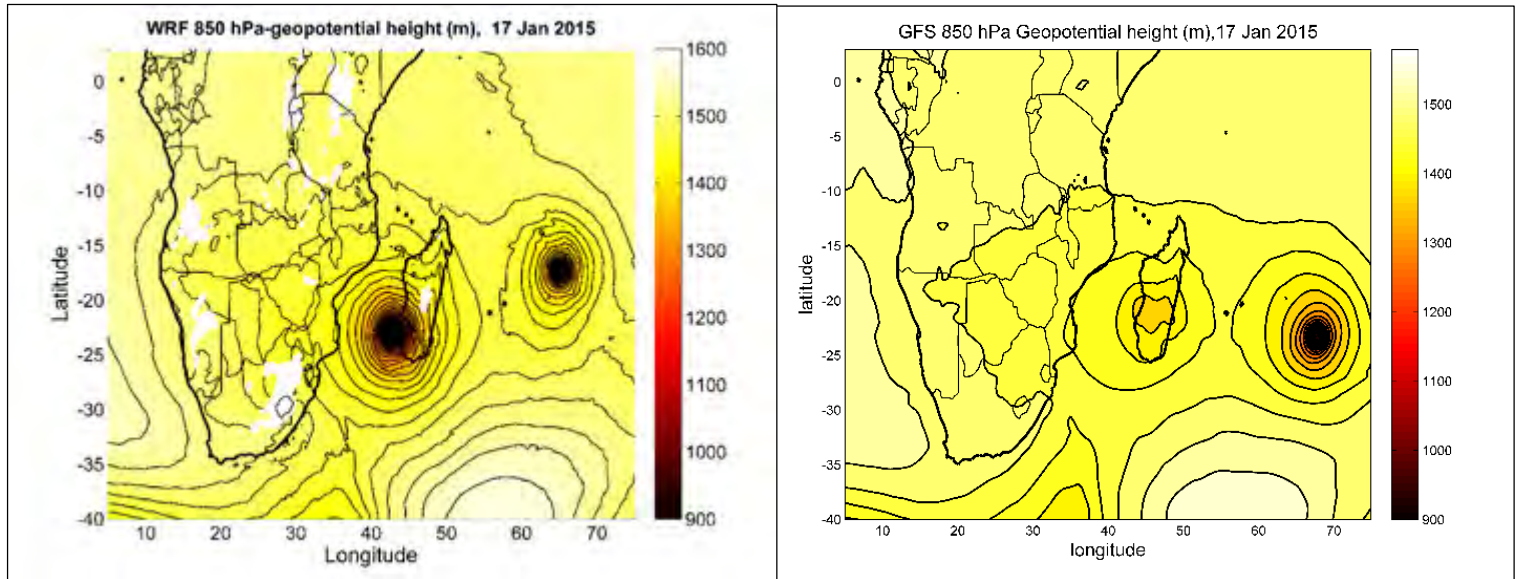
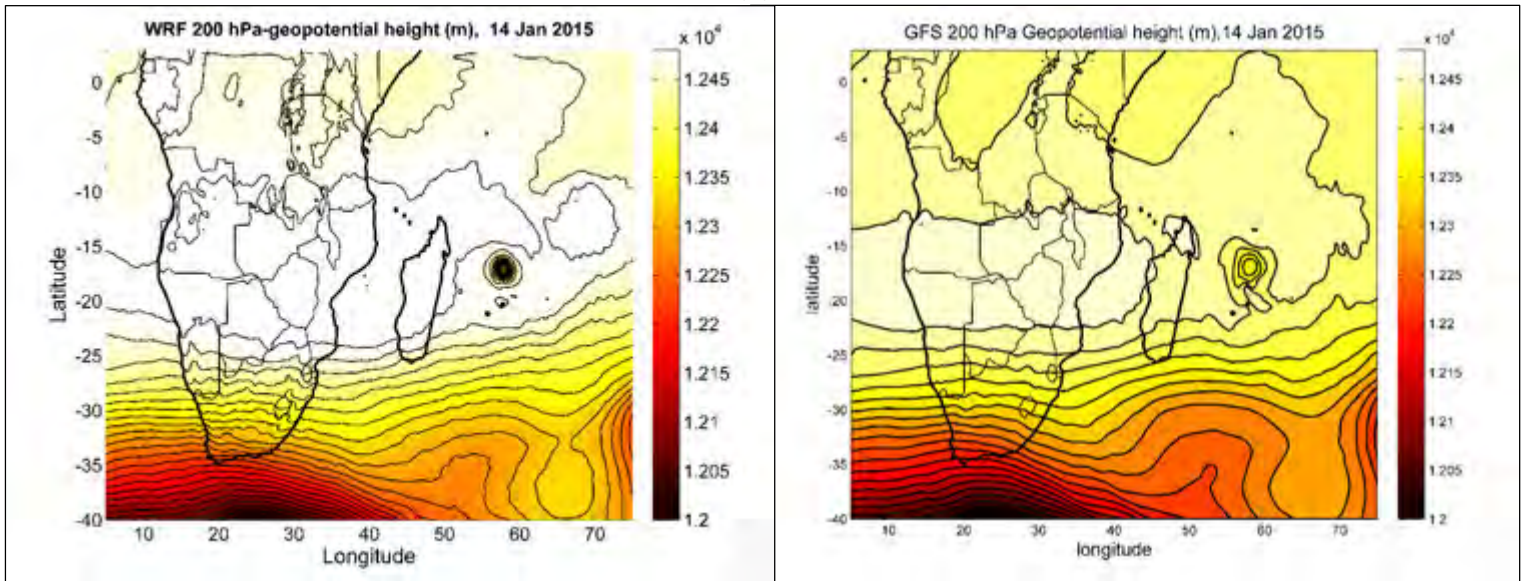


Figure 7: (Continued) 850 hPa geopotential height (m) comparison between WRF simulation (left) and GFS analyses from (a) 14 to (d) 17 January 2015 at 0000 UTC. Contour interval is 20 m.

(a)



(b)

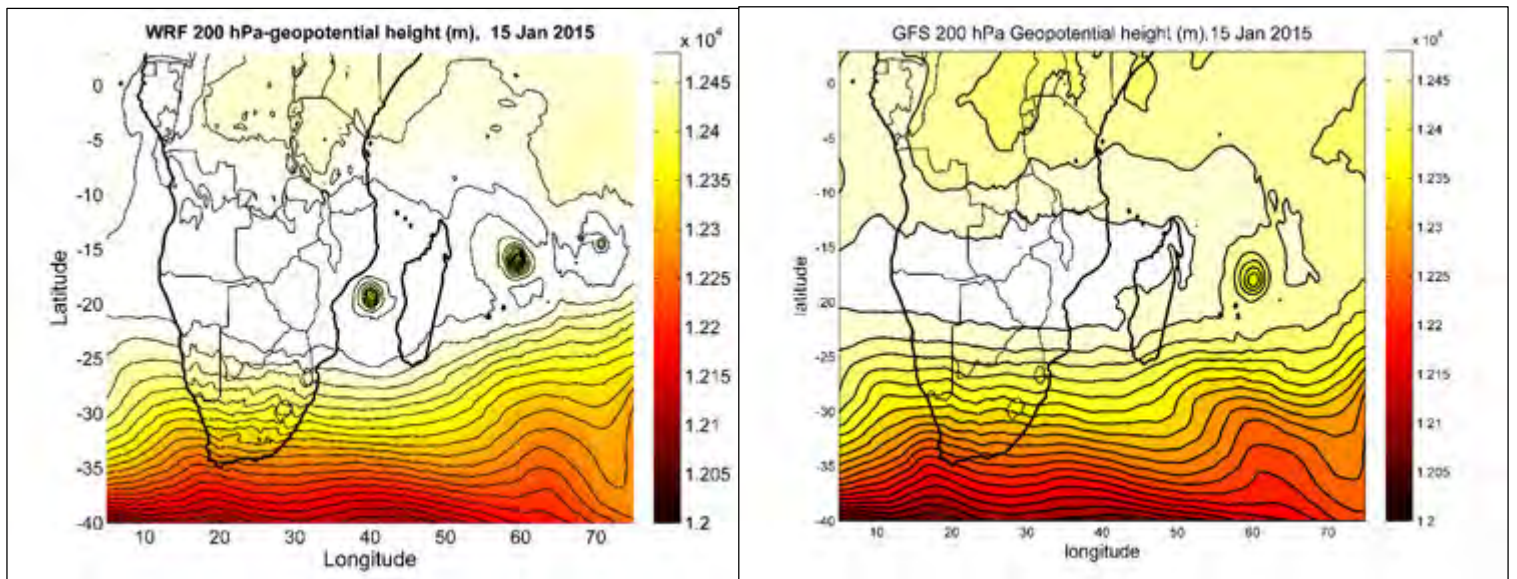
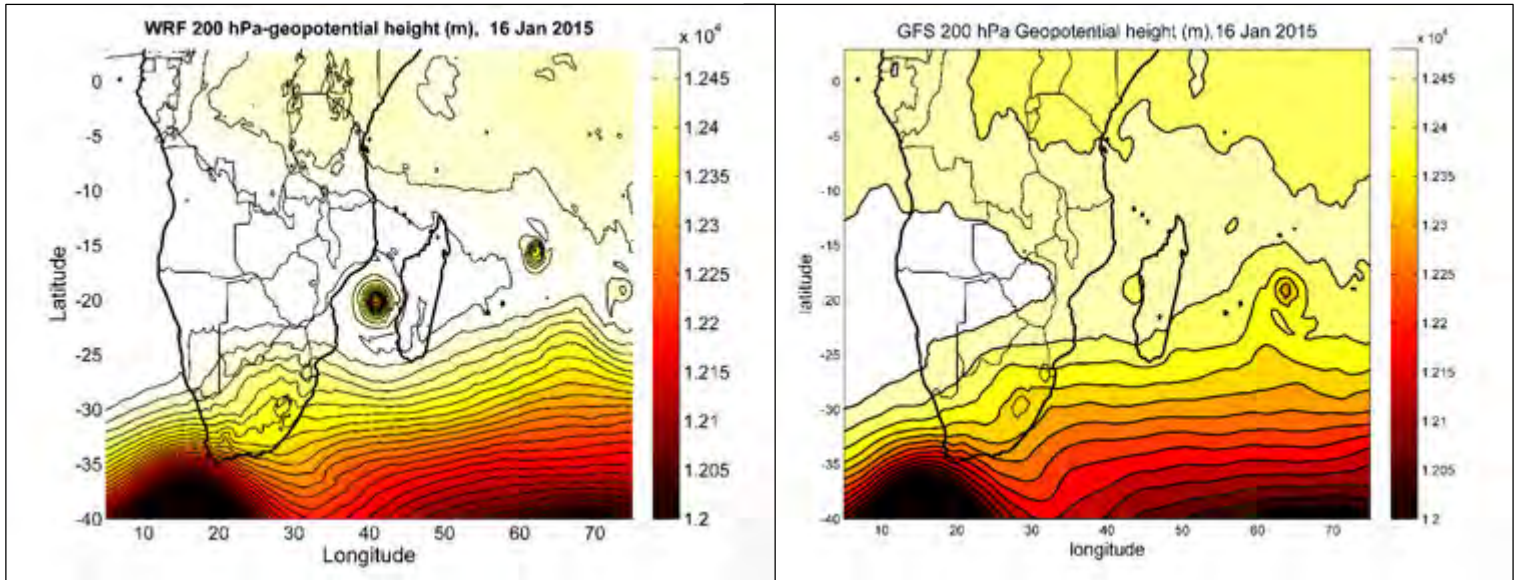


Figure 8: 200 hPa geopotential height (m) comparison between WRF simulation (left) and GFS analyses from (a) 14 to (d) 17 January 2015 at 0000 UTC (Continued on next page). Contour interval is 20 m.

(c)



(d)

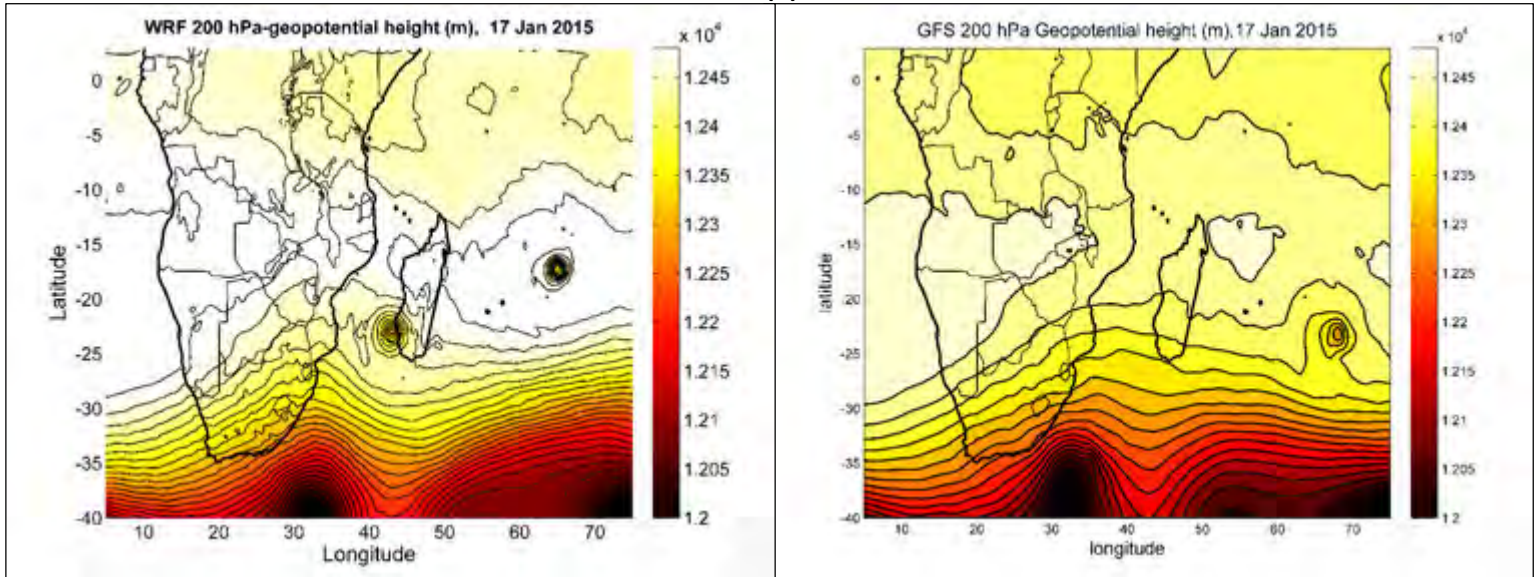


Figure 8: (Continued) 200 hPa geopotential height (m) comparison between WRF simulation (left) and GFS analyses from (a) 14 to (d) 17 January 2015 at 0000 UTC. Contour interval is 20 m.

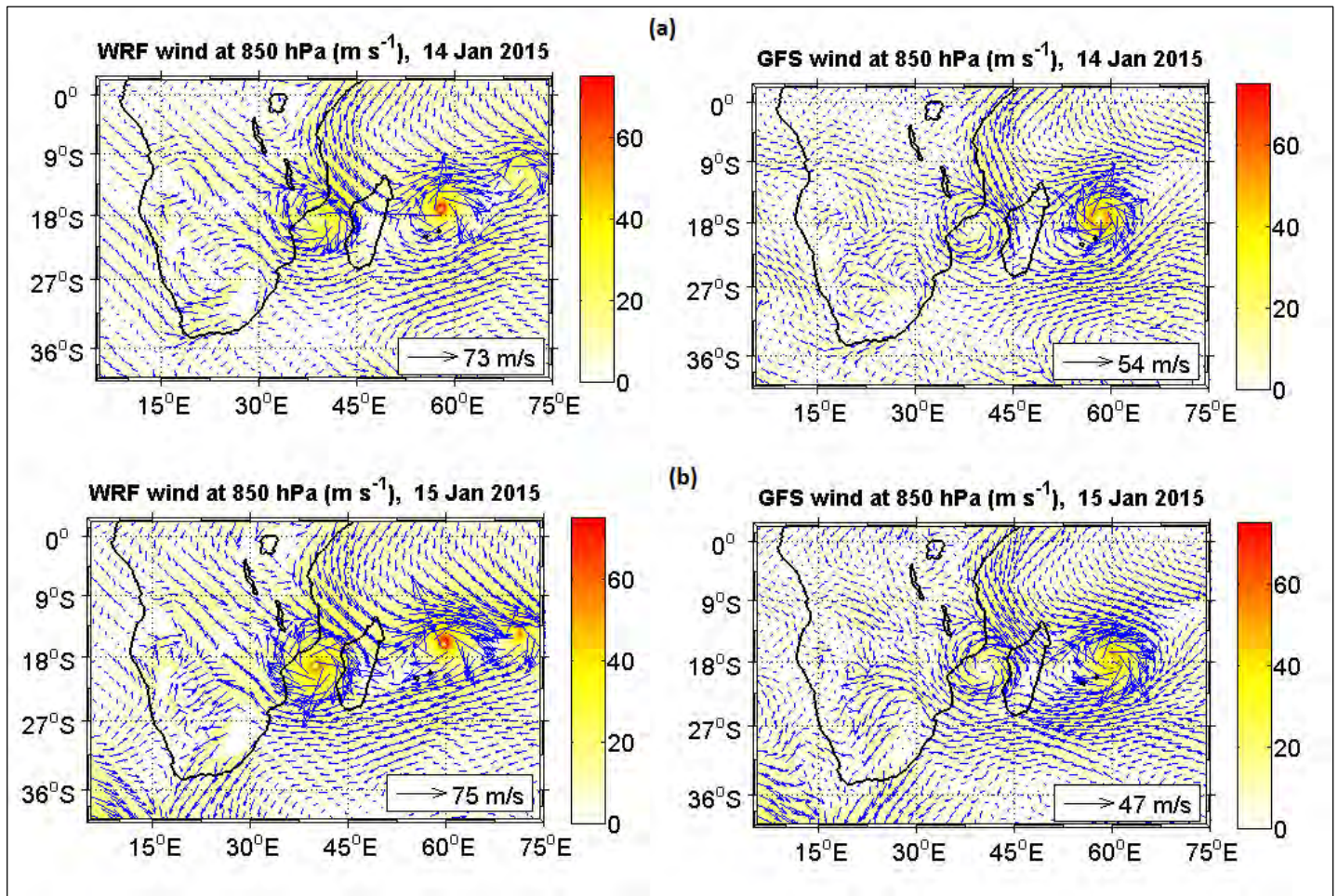


Figure 9: 850 hPa wind fields (m s^{-1}) comparison between WRF model simulation (left) and GFS analyses (right) from (a)14 to (d)17 January 2015 at 0000 UTC (Continued on next page).

The arrow in the bottom right of each panel denotes maximum wind speed.

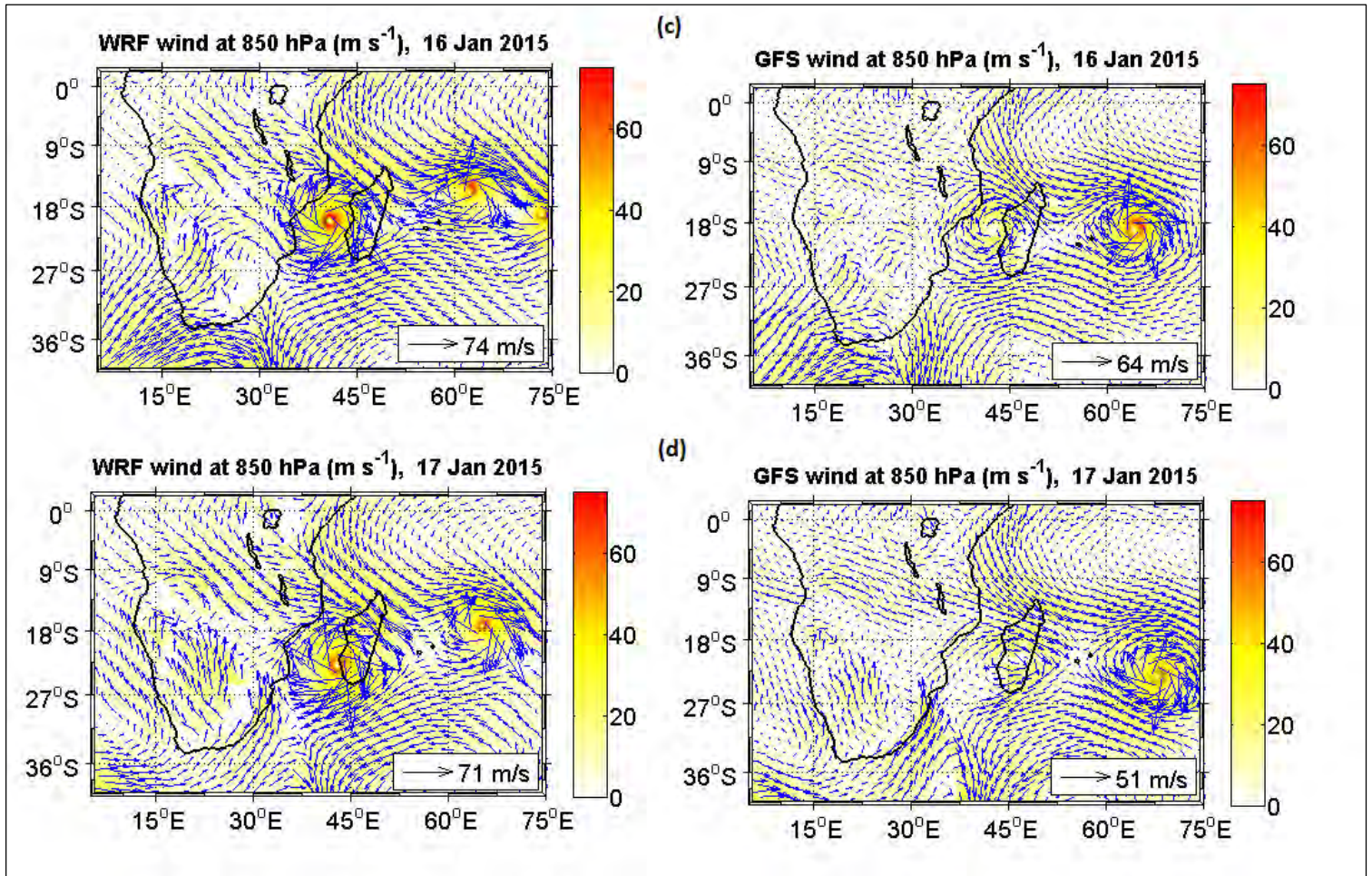


Figure 9: (Continued) 850 hPa wind fields (m s^{-1}) comparison between WRF model simulation (left) and GFS analyses (right) from (a)14 to (d)17 January 2015 at 0000 UTC. The arrow in the bottom right of each panel denotes maximum wind speed.

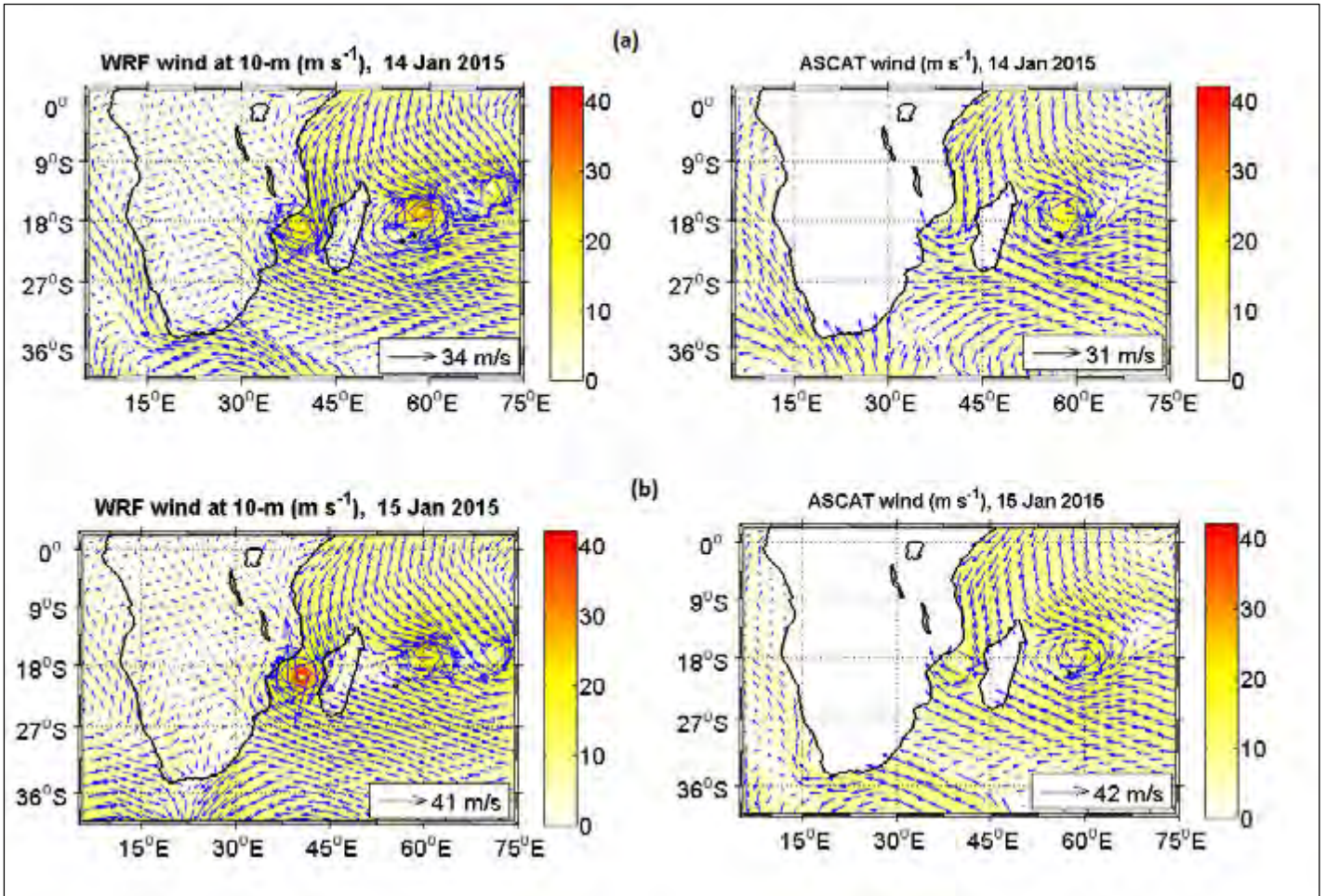


Figure 10: Daily surface wind fields (m s^{-1}) comparison between 10-m WRF wind (left) and ASCAT wind (right) from (a) 14 to (d) 17 January 2015 (Continued on next page). The arrow in the bottom right of each panel denotes maximum wind speed.

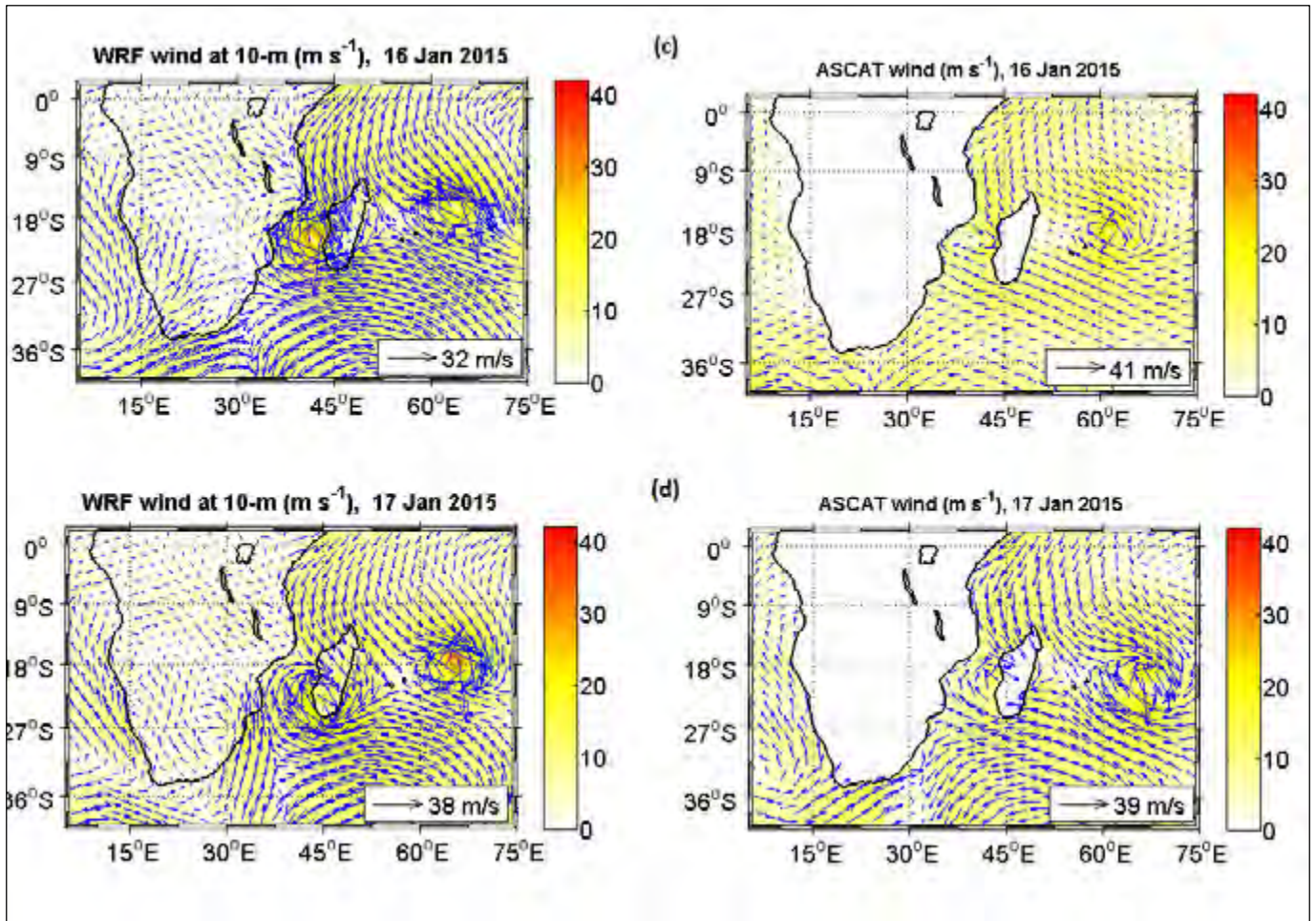


Figure 10: (Continued) Daily surface wind fields (m s^{-1}) comparison between 10-m WRF wind (left) and ASCAT wind (right) from 14 to 17 January 2015. The arrow in the bottom right of each panel denotes maximum wind speed.

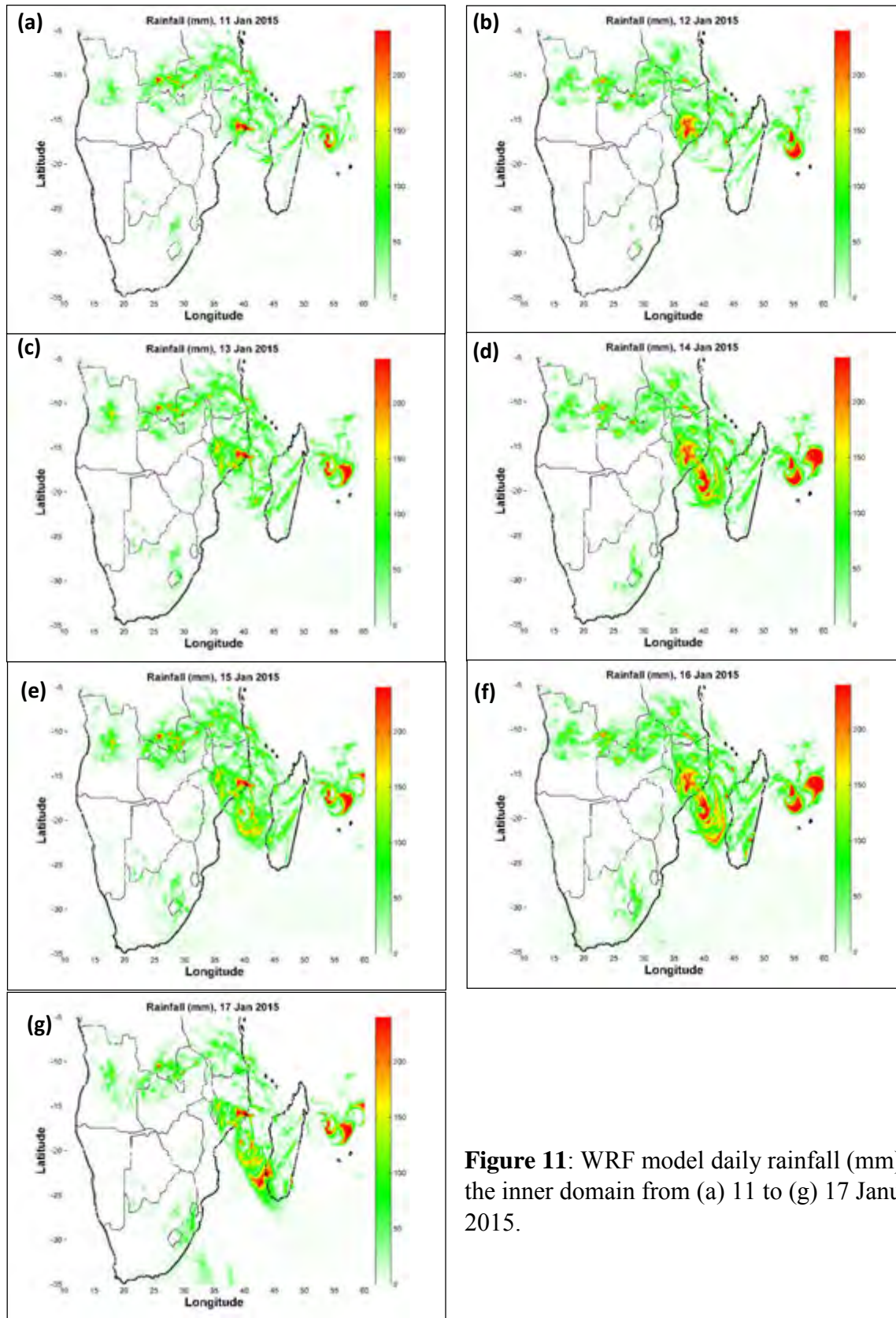


Figure 11: WRF model daily rainfall (mm) over the inner domain from (a) 11 to (g) 17 January 2015.

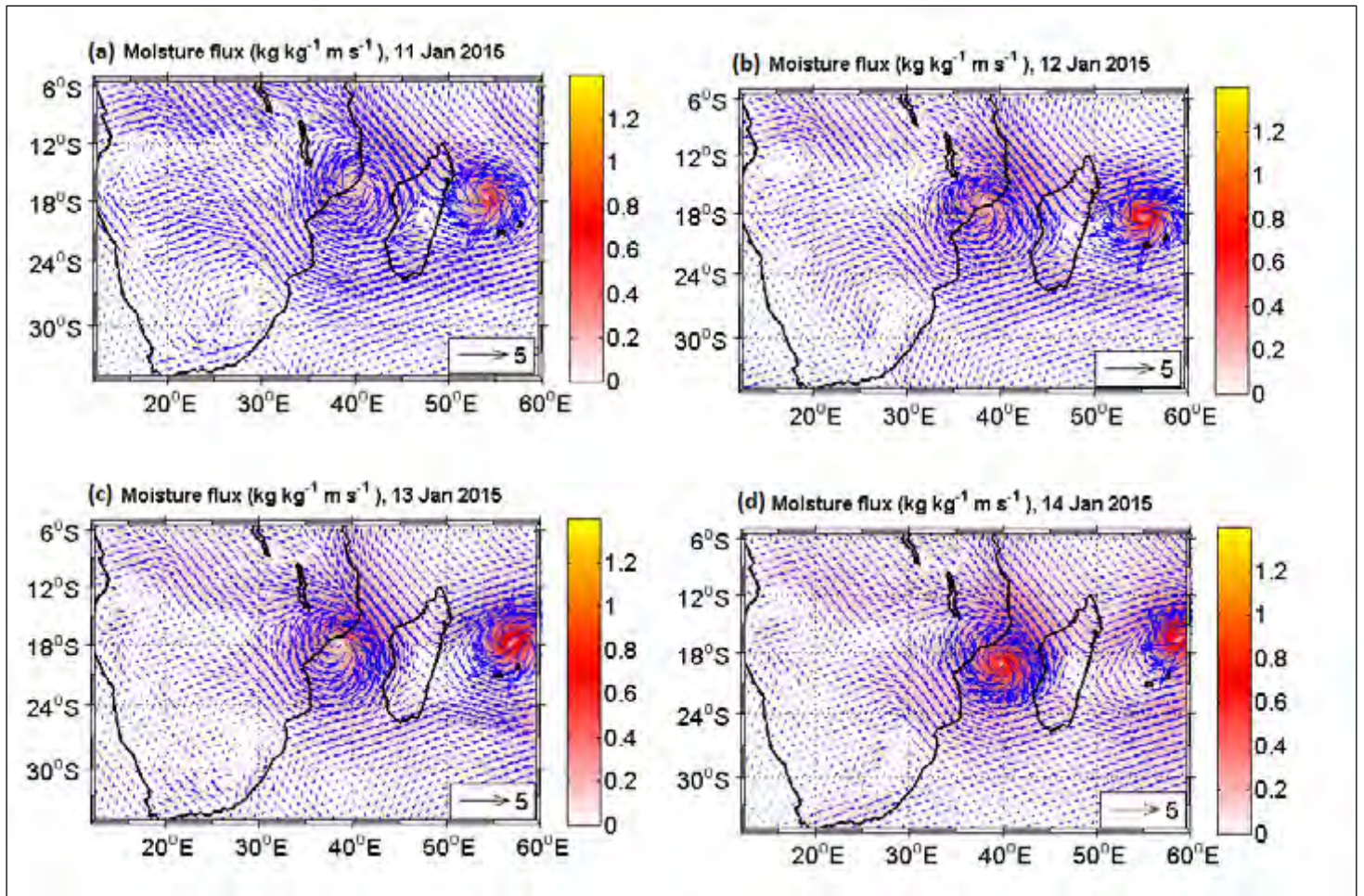


Figure 12: WRF model daily moisture flux (shaded, $\text{kg kg}^{-1} \text{m s}^{-1}$) at 850 hPa from (a) 11 to (g) 17 January 2015 (Continued on next page). Note that for data the values were not plotted at each model grid point. The arrow in the bottom right of each panel denotes the scale which has been used to make the vectors more visible. The actual magnitude of the flux is given in the colour bar.

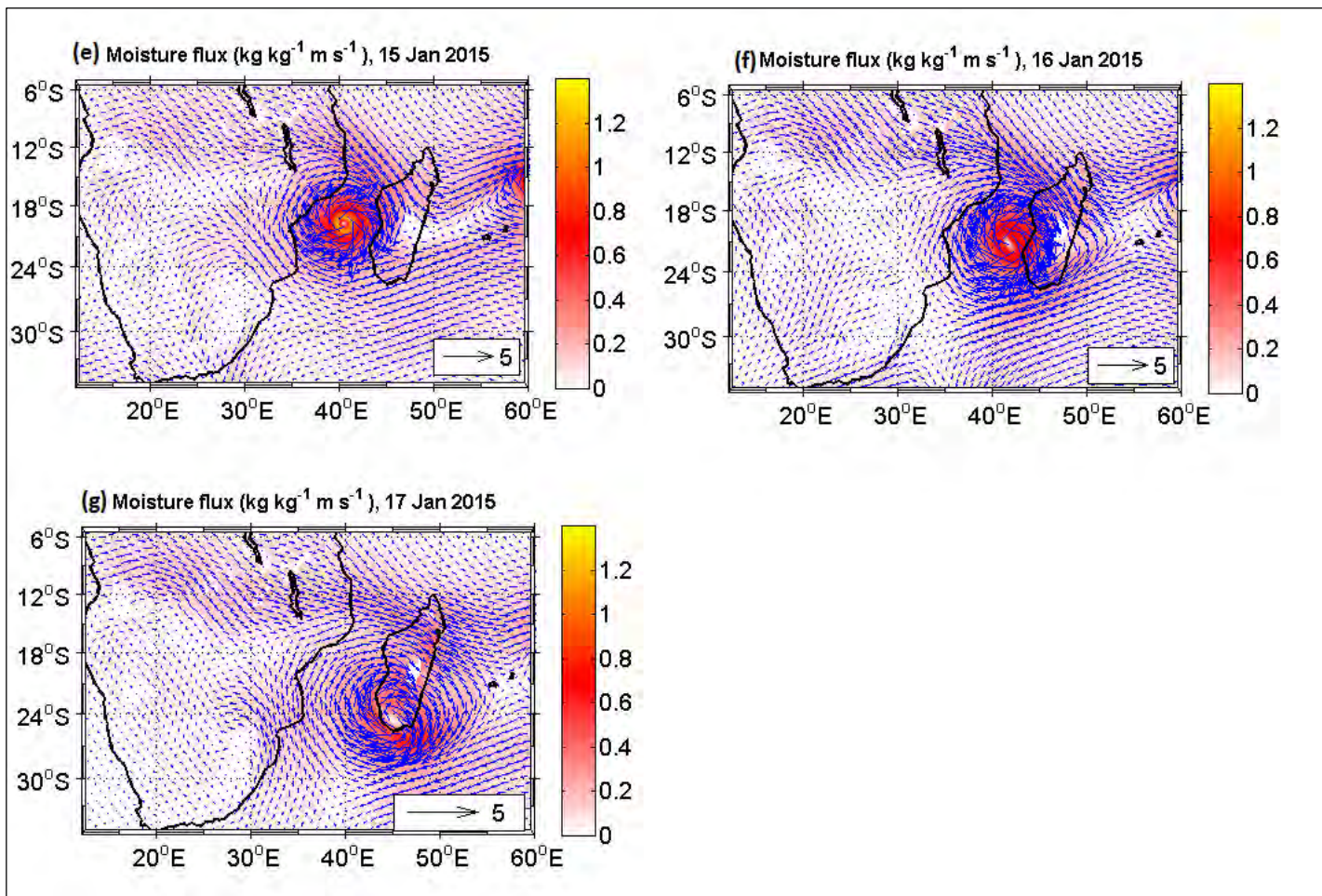


Figure 12: (Continued) WRF model daily moisture flux (shaded, $\text{kg kg}^{-1} \text{m s}^{-1}$) at 850 hPa from (a) 11 to (g) 17 January 2015. Note that for data the values were not plotted at each model grid point. The arrow in the bottom right of each panel denotes the scale which has been used to make the vectors more visible. The actual magnitude of the flux is given in the colour bar.

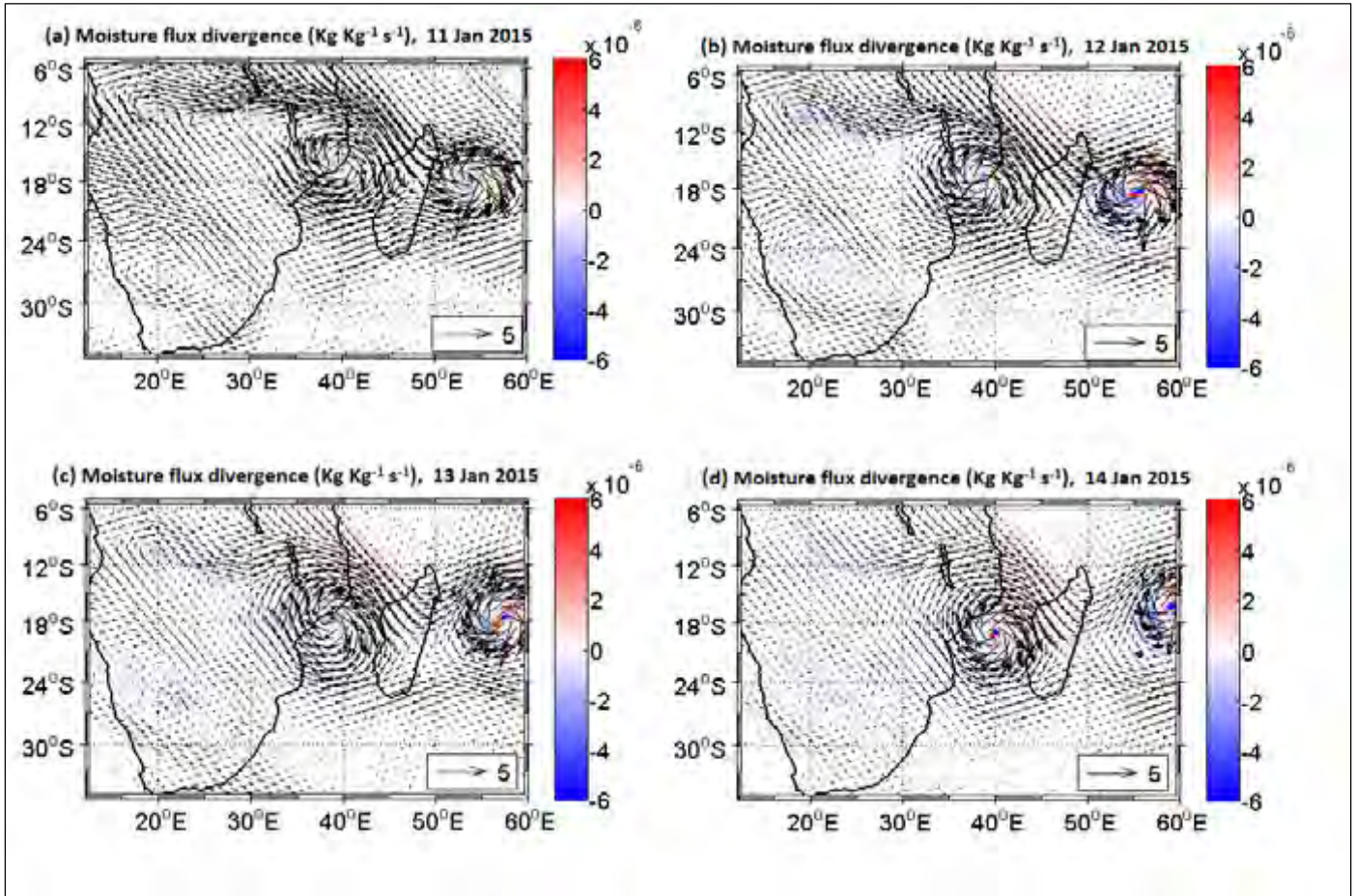


Figure 13: WRF model daily moisture flux divergence (shaded, $\text{kg kg}^{-1} \text{s}^{-1}$) at 700 hPa from (a) 11 to (g) 17 January 2015 (Continued on next page). Negative (positive) values imply convergence (divergence). Note that for data the values were not plotted at each model grid point. The arrow in the bottom right of each panel denotes the scale which has been used to make the vectors more visible. The actual magnitude of the flux is given in the colour bar.

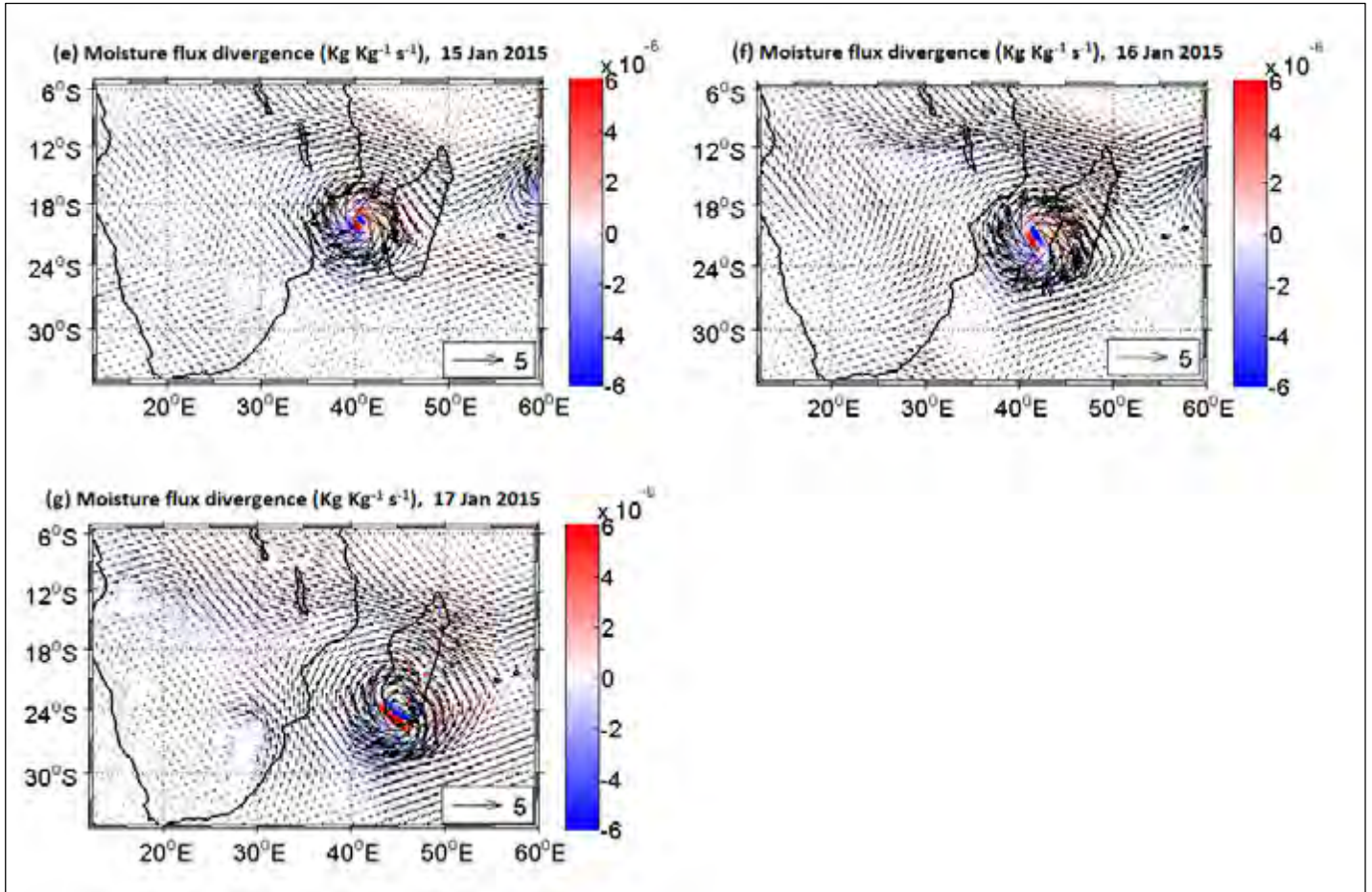


Figure 13: (Continued) WRF model daily moisture flux divergence (shaded, $\text{kg kg}^{-1} \text{s}^{-1}$) at 700 hPa from (a) 11 to (g) 17 January 2015. Negative (positive) values imply convergence (divergence). Note that for data the values were not plotted at each model grid point. The arrow in the bottom right of each panel denotes the scale which has been used to make the vectors more visible. The actual magnitude of the flux is given in the colour bar.

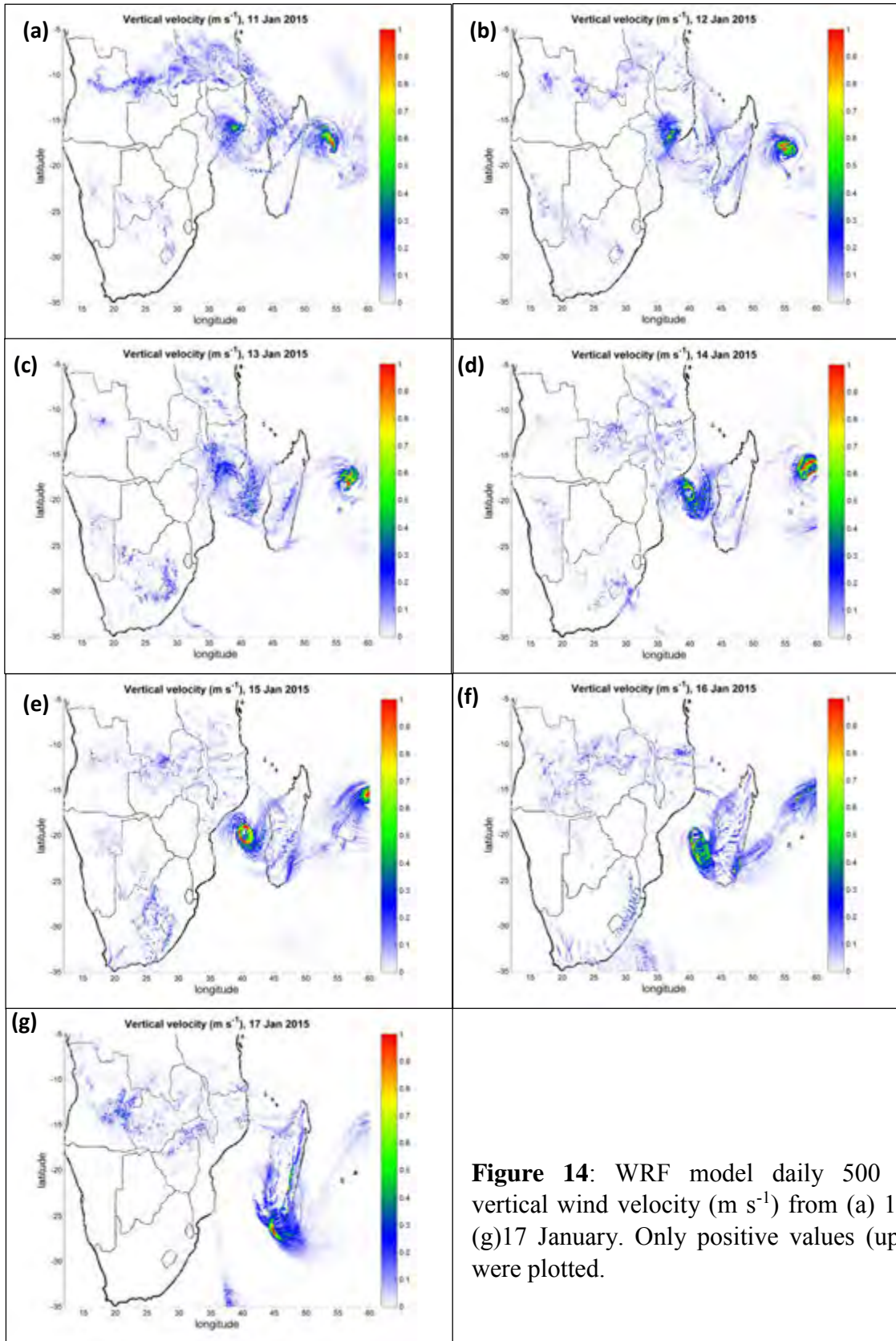


Figure 14: WRF model daily 500 hPa vertical wind velocity (m s⁻¹) from (a) 11 to (g) 17 January. Only positive values (uplift) were plotted.

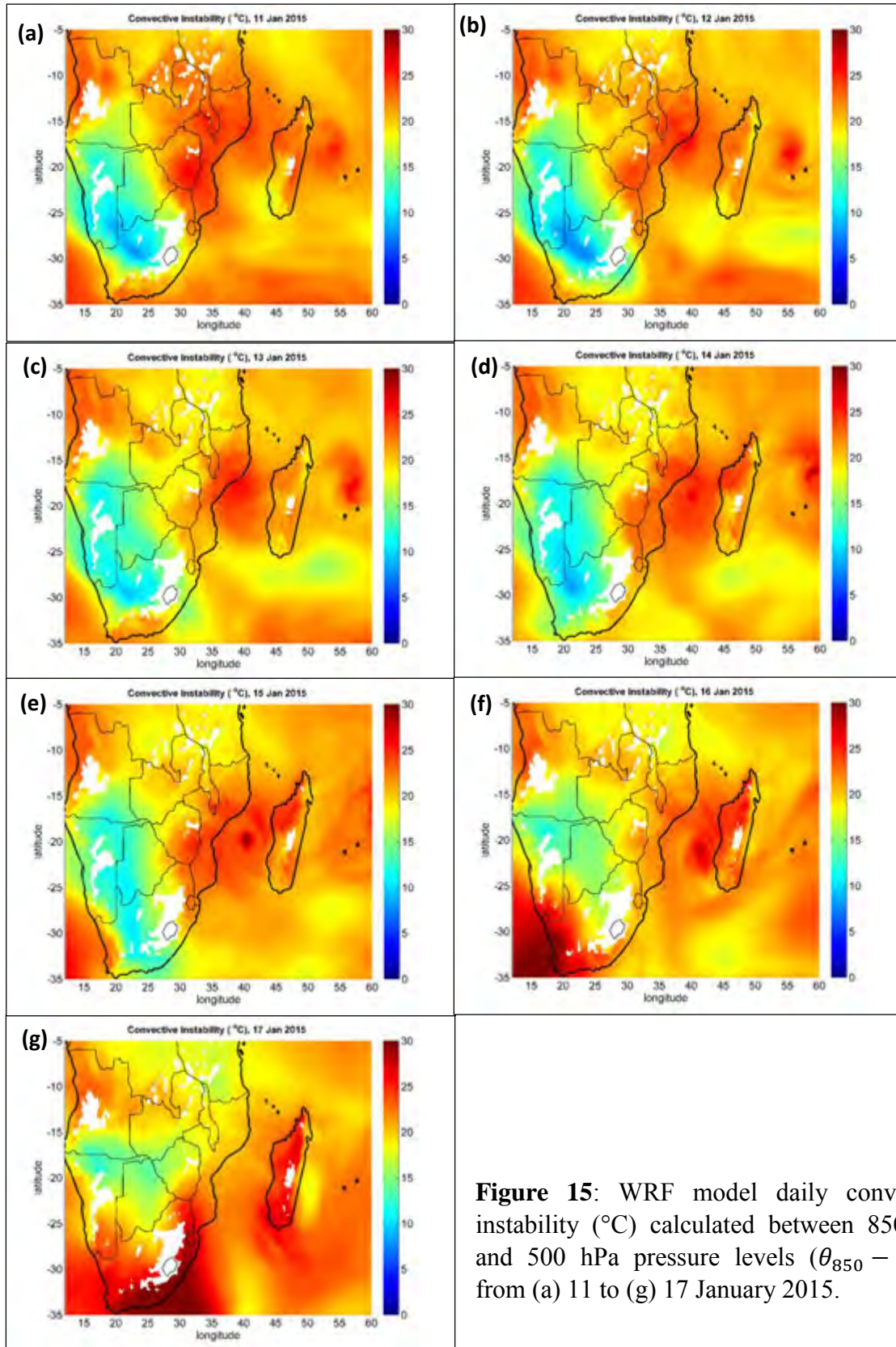


Figure 15: WRF model daily convective instability ($^{\circ}\text{C}$) calculated between 850 hPa and 500 hPa pressure levels ($\theta_{850} - \theta_{500}$) from (a) 11 to (g) 17 January 2015.

Chapter 5

5. Conclusions

In this study, tropical storm Chedza (11-17 January 2015) which developed over the Mozambique Channel has been investigated using the WRF model, satellite data sets (TRMM and ASCAT), and station rainfall data. Motivation for studying Chedza follows from the fact this storm resulted in heavy rainfall over Mozambique, southern Malawi and southern Madagascar. It produced well over 50% of the January 2015 rainfall at several Mozambican stations (Table 2) and led to flooding in several areas, not only causing marked damage, but also the loss of life. The main aim of this study was to analyse a WRF model simulation of this event and see whether the model fields could be used to better understand the mechanisms associated with the heavy rainfall that occurred over Mozambique between 11 and 17 January. A comparison of WRF winds, circulation, and rainfall with GFS analyses, ASCAT satellite derived winds and TRMM rainfall gave confidence in the ability of WRF to adequately represent the event.

The model fields indicated that regions of low-level moisture flux convergence, mid-level uplift, and convective instability, were consistent with those of heavy rainfall. Over northern Mozambique, convergence between the circulation associated with Chedza with that due to the monsoonal northwesterlies contributed to the heavy rainfall there during the first few days of the period. Orographic effects played a role in enhancing the rainfall near Cuamba/southern Malawi on the 12-14 January and in southwestern Madagascar during 15-17 January. The presence of an unstable air mass over Mozambique during this period also contributed to the rainfall.

The general flow patterns for the period 11 to 17 January were adequately simulated with the WRF model. However, there were some discrepancies in the model, particularly in terms of the position of the storm, its movement and direction. Other discrepancies included the intensity, in terms of maximum wind speed and the minimum central core pressure, compared to GFS and ASCAT winds. The 850 hPa geopotential height WRF compared well with the GFS analyses pressure patterns, except that there were some obvious discrepancies in the position of tropical storm Chedza on 17 January 2015. Also, the model generated an additional small cyclone east of Bansi, which was absent in GFS analyses but evidence of such a feature in the ASCAT satellite derived winds. It could be suggested that the additional cyclone east of Madagascar evident in Chedza may be due to higher resolution in WRF (6.67 km resolution over the inner domain) which is able to better resolve and capture small-scale features than the GFS analyses. The WRF simulated surface winds at 10 m above the surface over the outer domain (20 km horizontal resolution) compared well with the 0.25° resolution ASCAT satellite derived wind. However, ASCAT tended to show weaker winds than WRF in the regions of Chedza and Bansi. Generally, however, the model appeared to reproduce the characteristics of tropical storm Chedza reasonably well compared to available observations.

It should be noted that WRF tended to over-estimate the rainfall compared to TRMM. Some of this discrepancy may result from the much higher resolution of the WRF output which might resolve local features better. However, the effects of local surface changes that may help explain some of the station rainfall amounts in **Fig. 5** were not explicitly considered. It is possible that the land surface or boundary layer parameterizations could be changed in WRF to improve the model representation of the rainfall. A major difference between WRF and GFS that remains to

be resolved concerns the obvious difference in the location of Chedza on 17 January in WRF compared to GFS and ASCAT. However, it should be noted that these latter two datasets also do not agree in the position of Chedza on this day and thus, it remains unclear as to which of WRF, GFS or ASCAT are more accurate in their positioning of Chedza as it dissipated in 17 January 2015.

References

- Astier, N., Plu, M., Claud, C. (2012). Associations between tropical cyclone activity in the South West Indian Ocean and El Niño Southern Oscillation, *Atmospheric Science Letters*, **16**: 506-511
- Behera, S.K., Yamagata, T. (2001). Subtropical SST dipole events in the southern Indian Ocean. *Geophysical Research Letters*, **28**(2), 327-829
- Blamey, R.C., Reason, C. J.C., (2012). Mesoscale Convective Complexes over Southern Africa. *Journal of Climate*, **25**, 753-766.
- Blamey, R.C., Reason, C.J.C., (2013). The Role of Mesoscale Convective Complexes in Southern Africa Summer Rainfall. *Journal of Climate*, **26**, 1654-1668.
- Brasby, J., Diab, R. D. (1995). Total ozone and synoptic weather relationships over southern Africa and surrounding oceans. *Journal of Geophysical Research*, **100**, 3022-3032.
- Bi, L., Jung, J.A., Morgan, M.C., Le Marshall, J.F. (2011). Assessment of Assimilating ASCAT Wind Retrievals in the NCEP Global Data Assimilation System. *Monthly Weather Review*, **139**, 3405-3421
- Cha, D.-H, Wang, Y. (2012). A Dynamical Initialization Scheme for Real-Time Forecasts of Tropical Cyclones Using the WRF Model. *Monthly Weather Review*, **141**, 964-986
- Cook, C., Reason, C. J.C., Hewitson, B. C. (2004). Wet and dry spell within particularly wet and dry summers in the South African summer rainfall region. *Climate Research*, **26**, 17-31.
- Crimp, S. J., Mason, S.J. (1999). The Extreme Precipitation of 11 to 16 February 1996 over South Africa. *Meteorology and Atmospheric Physics*, **70**, 29-42.
- Dudhia, J. (1989), Numerical study of convection observed during the winter monsoon experiment using a mesoscale two-dimensional model. *Journal of Atmospheric Science*, **46**, 3077-3107.
- Dyson, L.L., van Heerden, J. (2001). The heavy rainfall and floods over the northeastern Interior of South Africa during February 2000. *South African Journal of Science*, **97**, 80-86.
- Ebert, E.E., Janowiak, J.E., Kidd, C. (2007). Comparison of Near-Real-Time Precipitation Estimates from Satellite observations and Numerical Models. *American Meteorological Society*. 47-64

- Figa-Saldana, J., Wilson, J.W., Attema, E., Gelsthorpe, R., Drinkwater, M.R., Stoffelen, A. (2002). The advanced scatterometer (ASCAT) on the meteorological operational (MetOp) platform: A follow on the European wind scatterometer. *Canadian Journal of Remote Sensing*, **28** (3), 404-412.
- Fitchett, J.M., Grab, S.W. (2014). A 66-year tropical record for south-east Africa: temporal trends in a global context. *International Journal of Climatology*, **34**. 3604-3614.
- Flesch, T.K., Reuter, G.W. (2012). WRF model simulation of Two Alberta flooding events and the impact of topography. *Journal of Hydrometeorology*, **13**, 695-708.
- Hansingo, K., Reason, C. J.C. (2009). Modelling the atmospheric response over southern Africa to SST forcing in the southeast tropical Atlantic and southwest subtropical Indian Ocean. *International Journal of Climatology*, **29**(7), 1001-1012.
- Harrison, M.S. (1984). A generalized classification of South African rain-bearing synoptic system. *International Journal of Climatology*, **4**, 547-560.
- Hart, N. C., Reason, C. J.C., Fauchereau, N. (2010). Tropical-Extratropical Interaction over Southern Africa: Three Cases of Heavy Summer Rainfall. *Monthly Weather Review*, **138**, 2608-2623.
- Henderson-Sellers, Z. H., Berz, G., Emanuel, K. G., Lansea, C., Holland, G., Lighthill, J., Weester, P. (1998). Tropical cyclones and global climate change: A post-IPCC assessment. *Bulletin of the American Meteorological Society*, **79**, 19-38.
- Hill, K. A., Lackmann. F. M. (2009). Influence of environmental humidity on tropical cyclone size. *Monthly Weather Review*, **137**, 3294-3315
- Hong, S.-Y., Dudhia., J., Chen, S.-H. (2004). A revised approach to ice microphysical processes for bulk parameterization of clouds and precipitation, *Monthly Weather Review*, **132**, 103-120.
- Hong, S.-Y., Lim, J.-O. J. (2006). The WRF Single-Moment 6-Class Microphysics Scheme (WSM6). *Journal of Korean Meteorological Society*, **42** (2), 121-151.
- Hong, S.-Y., Lee, J.-W. (2009). Assessment of the WRF model in reproducing a flash-flood heavy rainfall event over Korea. *Atmospheric Research*, **93**, 818-831.
- Ibrahim, S., Afandi, G. (2014). Short-range Rainfall Prediction over Egypt using the Weather Research and Forecasting Model, *Open Journal of Renewable Energy and Sustainable Development*, **1**, 56-70
- Islam, T., Srivastava, P. K., Rico-Ramirez, M. A., Dai, Q., Gupta, M., Singh, S. (2015). Tracking a tropical cycle trough WRF-ARW simulation and sensitivity of model physics. *Natural Hazards*, **76**, 1473-1495.

- Jiang, H., Halverson, J.B., Simpson, J. (2008) On the Differences in Storm Rainfall from Hurricanes Isidore and Lili. Part I: Satellite Observations and Rain Potential. *Weather and Forecasting*, **23**, 29-43.
- Jury, M. R. (1996). Regional teleconnection patterns associated with summer rainfall over South Africa, Namibia, and Zimbabwe. *International Journal of Climatology*, **16**, 135-153.
- Jury, M. R., Pathack, B., Parker, B. (1999). Climatic determinants and statistical prediction of tropical cyclone days in the southwest Indian Ocean. *Journal of Climate*, **12**(6), 1738-1746.
- Kain, J.S. (2004). The Kain-Fritsch convective parameterization: an update. *Journal Applied of Meteorology*, **43**, 170-181.
- Kalnay, E., M. Kanamitsu, R. Kistler, W. Collins, D. Deavan, L. Gandin, M.-I redell,-S .. - Sarah,-G. WhiterK. Woollen, Y. Zhu, M. Chelliah, W. Ebisuzaki, W. Higgins, J. Janowiak, K.C. Mo, C. Ropolewski, J. Wang, A. Leetmaa, R. Reynolds, R. Jenne, and D. Joseph. (1996). The NCEP/NCAR 40-year reanalysis project. *Bulletin of the American Meteorological Society.*, **77**, 437-471.
- Kim, D., Jim., C., Ho.C., Kim, J., Kim, J. H. (2015). Climatological features of WRF-simulated tropical cyclones over the western North Pacific. *Climate Dynamics*, **44**, 3223-3235
- Klinman, M.G., Reason, C.J.C. (2008). On the peculiar storm track of TC Favio during the 2006-2007 Southwest Indian Ocean tropical cyclone season and relationships to enso. *Meteorology and Atmospheric Physics*, **100**, 233-242.
- Kumar, A., Dudhia, J., Rotunno, R., Niyogi, D., Mohanty, U.C. (2008). Analysis of the 26 July 2005 Heavy rainfall event using the Weather Research and Forecasting (WRF) model, *Quarterly Journal of Royal Meteorological Society*, **134**, 1897-1910.
- Lui, Z., Ostrenga, D., Teng, W., Kempler, S. (2012). Tropical Rainfall Mission (TRMM) Precipitation and Services for Research and Applications, *American Meteorological Society*, 1317-1325
- Lin, N., Smith, J.A., Villarini, G., Marchok, T.P., Baeck, M.L. (2010). Modelling extreme rainfall, winds, and surge from hurricane Isabel, *Weather and forecasting*, **25**, 1342-1361.
- Lyon, B., Mason, S.J. (2007). The 1997–98 summer rainfall season in southern Africa. Part I: Observations. *Journal of Climate*, **20**, 5134– 5148.
- Malan, N., Reason, C. J.C., Loveday, B. R. (2013). Variability in tropical cyclone heat potential over the Southwest Indian Ocean. *Journal of Geophysical Research*, **118**, 6734-6746.

- Malherbe, J., Engelbrecht, F. A. (2013). Projected changes in tropical cyclone climatology and landfall in the Southwest Indian Ocean region under enhanced anthropogenic forcing. *Climate Dynamics*, **40**, 2867-2886.
- Malherbe, J., Engelbrecht, F. A., Landman, W. A., Engelbrecht, C. J. (2012). Tropical systems from the southwest Indian Ocean making landfall over the Limpopo River Basin, southern Africa: a historical perspective. *International Journal of Climatology*, **32**, 1018-1032.
- Manhique, A.J., Reason, C.J.C., Silinto, B., Zucula, J., Raiva, I., Congolo, F., Mavume, A.F. (2015). Extreme rainfall and floods in southern Africa in January 2013 and associated circulation patterns. *Natural Hazards*, **77**, 679-691.
- Mason, S. (1995). Sea-surface temperature - South African rainfall associations, 1910-1989. *Journal of Climatology*, **15**(2), 119-135.
- Mason, S., Jury, M. (1997). Climatic variability and change over southern Africa: a reflection on underlying processes. *Progress in Physical Geography*, **21**(1), 23.
- Mawren, D., Reason, C.J.C. (2016). Variability of tropical cyclone heat potential and barrier layers in the South Indian Ocean. *Journal of Geophysical Research.*, under review
- Mavume, A. F., Rydberg, L., Rouault, M., & Lutjeharms, J. R. (2009). Climatology and Landfall of Tropical Cyclones in the Southwest Indian Ocean. *Western Indian Ocean Journal of Marine Science*, **8**(1), 15-36.
- Midgley, G.F., Chapman, R.A., Hewitson, B., Johnston, P., de Wit, M., Ziervoleg , G., Makheibir, P., van Niekerk, I., Tadross, M., van Wilgen, B.W., Kgope, B., Morant, P.D., Theron, A., Scholes, R.J., Forsyth, G.G. (2005). A Status Quo, Vulnerability and Adaptation Assessment of the Physical and Socio-economic Effects of Climate Change in The Western Cape. CSIR report.
- Nesbitt, S.W., Zipser, E.J., Kummerow, C.D. (2004). An examination of version 5 rainfall estimates from the TRMM microwave imager, precipitation radar, and rain gauges on global, regional, and storm scales. *Journal of Applied Meteorology*, **43**, 1016-1036.
- Nash, D.J., Pribyl, K., Klein, J., Endfield, G.H., Kniveton, D.R., Adamson, G.C. (2015). Tropical cyclone activity over Madagascar during the late nineteenth century. *International Journal of Climatology*, **35**, 3249-3261.
- Nieto, R., Sprenger, M., Trigo, R.M. (2008). Identification and Climatology of Cut-off Lows near the Troposphere. *Trend and Directions in Climate Research*, **252**, 257-287.
- Nguyen, L.T., Molinari, J., Thomas, D. (2014). Evaluation of tropical cyclone center identification methods in numerical models. *Monthly Weather Review*, **142**, 4326-4339.

- Noh, Y., Cheon, W.G., Hong, S.Y., Raasch. (2003) The improvement of K-profile model for the PBL using LES. *Boundary Layer Meteorology*, **107**, 401-427.
- Rafiq, L., Blaschke, T., Tajbar, S. (2015). Arabian Sea cyclone: Structure analysis using satellite data. *Advances in Space Research*, **56**, 2235-2247.
- Reason, C. J.C. (2001). Evidence for the influence of the Agulhas Current on regional atmospheric circulation patterns. *Journal of Climate*, **14**(12), 2769-2778.
- Reason, C.J.C. (2002). Sensitivity of the southern African circulation to dipole SST patterns in the South Indian Ocean. *International Journal of Climatology*, **22**, 377-393.
- Reason, C.J.C. (2007). Tropical cyclone Dera, the unusual 2000/01 tropical season in the southwest Indian Ocean and associated rainfall anomalies over Southern Africa. *Meteorology and Atmospheric Physics*, **97**, 181-188.
- Reason, C. J.C., Mulenga, H. (1999). Relationships between South African Rainfall and SST anomalies in the southwest Indian Ocean. *International Journal of Climatology*, **19**, 1651-1673.
- Reason, C. J.C., Keibel, A. (2004). Tropical Cyclone Eline and Its Unusual Penetration and Impacts over the Southern African Mainland. *Weather and Forecasting*, **19**, 789-805.
- Reason, C. J.C., Hachigonta, S., Phaladi, R. F. (2005). Interannual variability in rainy season characteristics over the Limpopo region of southern Africa. *International Journal of Climatology*, **25**, 1835-1853.
- Reason, C.J.C., Landman, W., Tennant, W. (2006). Seasonal to Decadal Prediction of Southern African Climate and Its Links with Variability of the Atlantic Ocean. *Bulletin of the American Meteorological Society*, **87**(7), 941-955.
- Reason, C. J.C, Smart, S. (2015). Tropical south east Atlantic warm anomalies over southern Africa. *Frontiers in Environmental Science*, **3**(24), 1-11.
- Reynolds, R.W., Smith, T. M., Lui, C., Chelton, D. B., Casey, K. S., Schlax, M. G. (2007). Daily high-resolution blended analyses for sea surface temperature. *Journal of Climate*, **20**, 5473-5496.
- Rouault, M., Florenchie, P., Fauchereau, N., Reason, C.J.C. (2003a). South east tropical Atlantic warm events and southern African rainfall. *Geophysical Research Letters*, **30**, 8009-8013.
- Rouault, M., Reason., C.J.C., Lutjeharms, J.R.E., Beljaars, A. (2003b). Underestimation of latent and sensible heat fluxes above the Agulhas Current in NCEP and ECMWF analyses. *Journal of Climate*, **16**, 776-782.

- Rouault, M., Fauchereau, N., Pohl, B., Penven, P., Richard, Y., Reason, C.J.C., Pegram, G.G.S., Phillippon, N., Siedler, G., Murgia, A. (2010). Multidisciplinary analysis of hydroclimatic variability at the catchment scale. *Water Research Commission Report No.1747/1/10*, 1-88.
- Singleton, A. T., Reason, C. J.C. (2007). A numerical Model study of an intense Cut-off Low Pressure over South Africa. *Monthly Weather Review*, **135**, 1128-1149.
- Skamarock, W.C., Klemp, J.B., Dudhia, J., Gill, D.O., Barker, D.M., Wang, W., Powers, J.G. (2005). A description of the Advanced Research WRF version.2 Note Tech NCAR/ TN-468+STR, 88.
- Skamarock, W.C., Klemp, J.B., Dudhia, J., Gill, D.O., Barker, D.M., Duda, M.G., Huang, X.Y., Wang, J.G. (2008). A description of the Advanced Research WRF Version 3. NCAR/TN-475 STR, NCAR Technical Note, Mesoscale and Microscale Meteorology Division, National Center for Atmosphere Research, June 2008, 133.
- Taljaard, J. J. (1985). Cut-off lows in the South African Region. *South African Weather Tech*, **14**, 153.
- Todd, M.C., Washington, R. (1998). Extreme daily rainfall in southern African and southwest Indian Ocean tropical temperate links. *South African Journal of Science*, **94**,64–70.
- Tyson, T. E., Dyer , T.G.J., Mametse, M.N. (1975). Secular changes in South African rainfall: 1880 to 1972, *Quarterly Journal of the Royal Meteorological Society*, **101**(430), 817-833
- Tyson, P. D., Preston-Whyte, R. S. (2015). *The Weather and Climate of Southern Africa* (2 ed.). Cape Town: Oxford University Press Southern Africa.
- Usman, M. T., Reason, C. J.C. (2004). Dry spell frequencies and their variability over southern Africa. *Climate Research*, **26**, 199-211.
- Walker, N.D., Mey, R.D. (1988). Ocean/atmosphere heat fluxes withing the Agulhas Retroflection Region. *Journal of Geophysical Research*, **93**,15473-15483.
- Washington, R., Preston, A. (2006). Extreme wet years over southern Africa: Role of Indian Ocean sea surface temperature, *Journal of Geophysical Research*, **111**, 1-15.

<http://disc.sci.gsfc.nasa.gov> [Accessed 3 June 2015]

<http://www.nhc.noaa.gov/aboutsshws.php> [Accessed 28 August 2015]

<https://www.dwa.gov.za/hydrology/weather.htm> [Accessed 11 November 2015]

<https://podaac.jpl.nasa.gov/dataset/ASCATB-L2-25km> [Accessed 5 July 2016]